Anticipatory adjustment of mechanical properties for motor stabilisation

Charlotte Le Mouel[1], Romain Brette[2]

1. corresponding author charlotte.lemouel@normale.fr, Max Planck Institute of Intelligent Systems

2. Sorbonne Université, INSERM, CNRS, Institut de la Vision, 17 rue Moreau, F-75012 Paris, France.

I. Abstract

External perturbation forces may compromise the success in a motor task, such as using a tool or simply standing still. Unexpected perturbations are particularly challenging, because of the delays in the neural feedback control of movement. We present a generic model of stabilisation with neural delays. According to this model, body mechanical properties such as stiffness and inertia play a critical role for maintaining immobility despite external perturbations, since they determine the relative speed at which perturbations are amplified during the neural response delay. Stiffness and inertia may be adjusted through changes in muscle co-contraction and posture. We therefore propose a novel role of feed-forward motor control in providing robustness to perturbations: the anticipatory adjustment of mechanical properties for motor stabilisation. Our model thus predicts that when immobility or accuracy become critical, the nervous system should adjust the body mechanical properties so as to reduce this relative speed, and should additionally reduce neural feedback gains to prevent over-compensation. This model accounts for the strategy that subjects employ when standing in challenging balance conditions and when manipulating unstable tools.

II. Introduction

External perturbation forces may compromise the success in a motor task, such as using a tool (Rancourt & Hogan, 2001), or simply standing still (Le Mouel, Tisserand, Robert, & Brette, 2018). Theories of motor control typically distinguish between the roles of feed-forward motor control (Shadmehr & Mussa-Ivaldi, 1994) and feedback (Scholz & Schöner, 1999) in providing robustness to perturbations. Thus, when subjects performing reaching movements are subjected to repeated patterns of external forces, they gradually learn to anticipate on these forces, and counteract them precisely at the time they occur (Shadmehr & Mussa-Ivaldi, 1994). This feed-forward cancellation of perturbations allows them to achieve accurate, straight reaching movements. However it requires accurate knowledge of the external forces, and therefore only develops after extensive practice. Feedback control on the other hand acts in response to a sensed deviation from the desired movement. It can therefore correct for unexpected perturbations.

Current theories emphasise the role of the motor cortex in the feedback correction of unexpected perturbations. Thus, the spinal feedback correction of perturbations is reduced when standing in challenging balance conditions, such as when standing facing a cliff (Sibley, Carpenter, Perry, & Frank, 2007), when standing on a narrow support (Trimble & Koceja, 2001) or simply when closing the eyes (Pinar, Kitano, & Koceja, 2010). The classical interpretation for this reduction in the spinal contribution to balance is that, in challenging conditions, the control of balance is delegated to supra-spinal structures, such as the cortex, which may allow for a more refined control than the spinal cord (Llewellyn, Yang, & Prochazka, 1990). The motor cortex is also attributed a major role in the feedback stabilisation of arm movements (Pruszynski & Scott, 2012). The difficulty with this approach is that the neural feedback control of movement introduces delays. Thus, after a perturbation, the earliest change in muscular contraction is due to spinal feedback and occurs with a delay of several tens of milliseconds (Hammond, 1956). The change in force due to this muscle contraction is only observed after an additional 20 ms (Hammond, 1956). Responses involving the cortex have even longer delays than spinal feedback (Pruszynski & Scott, 2012). It is well known from control theory that delays are critical when using sensory feedback to counteract external perturbations (Aström & Murray, 2010): thus, a system that is stabilized by feedback control may become unstable

simply if the control delay increases. Relying on the cortex for feedback control would therefore increase instability. This may be particularly critical when faced with unexpected perturbations.

During this neural response delay after a perturbation, the movement of the body is entirely determined by the body and environmental mechanical properties, such as stiffness, inertia and weight. Recent advances in embodied robotics have demonstrated that stabilisation can be achieved by appropriately designing the robot mechanical properties, without the need for feedback control (Sproewitz et al., 2013). Thus, stability to changes in terrain height can be obtained by attaching springs in parallel to the joints of the robot's legs. This however requires the engineer to design the mechanical properties in view of a specific task: mechanics appropriate for walking may thus not be appropriate for stable stance (McGeer, 1990). This suggests that human motor versatility relies on the ability to adjust the body mechanics in view of the motor task. The literature in sports science indeed suggests that improvements in athletic performance rely on adjustments of muscle properties to the practiced sport (Duchateau & Baudry, 2010). Such changes in muscle mass or fatigue resistance occur over weeks or months. However changes in the body mechanical properties may also occur flexibly in anticipation of the motor task, through changes in posture (Le Mouel & Brette, 2017; Trumbower, Krutky, Yang, & Perreault, 2009) and muscle co-contraction (Nielsen, Sinkjær, Toft, & Kagamihara, 1994; Trimble & Koceja, 2001)

We thus propose a novel role of feed-forward motor control in providing robustness to perturbations: the anticipatory adjustment of mechanical properties for motor stabilisation. As stated previously, the role of feed-forward control for motor stabilisation is traditionally assumed to rely on accurate knowledge of the perturbation forces (Shadmehr & Mussa-Ivaldi, 1994). However, we present a model that demonstrates that the adjustment of body mechanical properties in advance of a perturbation can improve robustness, without the need for specific knowledge of the perturbation forces. This is achieved through changes in co-contraction or posture, to reduce the amplification of perturbations during the neural feedback delay. This adjustment must be coordinated with a decrease in neural feedback to prevent over-compensation. The decreased spinal gains observed during standing in challenging balance conditions should therefore not be interpreted as the mark of a more cortical control of balance, but on the contrary as the sign that motor stabilisation is achieved through the adjustment of mechanical properties. We also show that this model accounts for the stabilisation strategies adopted by subjects when manipulating unstable tools.

III. Modelling results

We first analyse a widely used model of human stance, the single inverted pendulum model presented in Figure 1 (Ian D. Loram, Maganaris, & Lakie, 2007).

1) Dynamics of the inverted pendulum during the neural response delay

When someone is standing on the ground, there are two external forces exerted on them: their weight and the ground reaction force (Figure 1). The point of application of the person's weight is called the centre of mass, noted CoM. The torque of weight around the person's ankles is thus $mg\mathrm{L}\sin(\Theta)$ (with m the person's mass, g gravity, L the CoM height and Θ the ankle angle). To understand the relative roles of body mechanical properties and feedback control in stabilisation, we decompose the ground reaction torque into a mechanical component $K(\Theta)$ due to ankle stiffness, which changes immediately upon a change in ankle angle, and a component C due to feedback muscle contraction with only changes after a delay τ_{delay} after a mechanical perturbation. The sum of the external torques affects the person's rotational momentum $J\dot{\Theta}$, where J is the rotational inertia around the ankles, according to the following equation:

$$J\ddot{\Theta} = m\,g\,L\sin(\Theta) - K(\Theta) - C$$

We consider that the person is initially at equilibrium at an angle Θ_0 with muscular contraction C_0, and linearize around this equilibrium, introducing θ, k, c such that:

$$\Theta = \Theta_0 + \theta$$
$$K(\Theta) = K(\Theta_0) + k\theta$$
$$C = C_0 + c$$

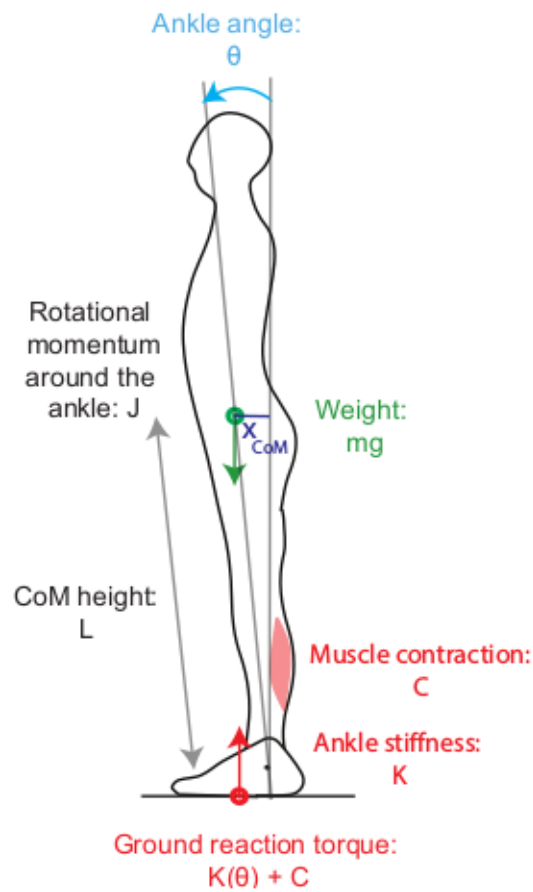

Figure 1 Single inverted pendulum model of stance (Loram et al. 2007). The external forces acting on the body are the weight (green arrow), whose torque around the ankle depends on ankle angle ϑ, and the ground reaction force (red arrow) whose torque depends on both ankle angle and muscle contraction

After linearization, the change in rotational momentum becomes:

$$J\ddot{\theta} = (mgLcos(\Theta_0) - k)\theta - c$$

During the response delay, the dynamics is therefore governed by the mechanical time constant τ_{mech}, defined by:

$$\tau_{mech} = \sqrt{\frac{J}{mgLcos(\Theta_0) - k}}$$

The combined effects of inertia J, stiffness k and environmental instability mg can thus be captured by their effect on this mechanical time constant. Any increase in ankle stiffness k up to $mgLcos(\Theta_0)$ increases the mechanical time constant of the body, and thus, as noted by Loram and colleagues, ankle stiffness slows down falling during the response delay (Ian D. Loram et al., 2007).

We can now reformulate the dynamical equation with respect to the time scale of neural intervention τ_{delay}:

$$\tau_{delay}{}^2\ddot{\theta} = S\theta - U(t - \tau_{delay})$$

where:

$$S = \frac{\tau_{delay}{}^2}{\tau_{mech}{}^2}$$

$$U = \tau_{delay}{}^2\frac{c}{J}$$

Thus, dynamics during the neural delay only depends a single dimensionless parameter S, which combines the effects of inertia, stiffness, environmental instability and feedback delay. This parameter captures how much perturbations are amplified during the feedback delay. This analysis shows that, for a given neural delay, it is advantageous to increase the mechanical time constant to slow down body dynamics, for example by stiffening the ankle.

2) Delayed feedback control of a pendulum

a. Delayed proportional-derivative controller

To characterise the influence of body mechanics on motor stabilisation, we must assume a particular type of feedback control. We choose the simplest possible feedback control that allows stability:

$$U = G\theta\left(t - \tau_{delay}\right) + D\tau_{delay}\,\dot{\theta}\left(t - \tau_{delay}\right)$$

This corresponds to the delayed version of the proportional-derivative controller, widely used for feedback control in engineering (Aström & Murray, 2010). This has been shown to correspond quantitatively to the contraction response of ankle muscles after a perturbation of stance (Welch & Ting, 2008). The damping term $D\tau_{delay}\,\dot{\theta}\left(t - \tau_{delay}\right)$ is necessary for stability because of the feedback delay. The control variable thus corresponds to a rudimentary form of anticipation:

$$\begin{aligned} U &= G(\theta\left(t - \tau_{delay}\right) + \frac{D}{G}\tau_{delay}\,\dot{\theta}\left(t - \tau_{delay}\right)) \\ &\approx G\theta(t - \tau_{delay} + \tfrac{D}{G}\tau_{delay}) \end{aligned} \tag{1}$$

Thus, the feedback control compensates for the delay when *D=G*.

b. Stability analysis

The dynamics of the controlled system are thus:

$$\tau_{delay}{}^2\ddot{\theta} - S\theta + G\theta\left(t - \tau_{delay}\right) + D\tau_{delay}\,\dot{\theta}\left(t - \tau_{delay}\right) = 0$$

We determine the feedback gains *(G,D)* which can stabilise a system of a given speed *S*, using the Nyquist criterion which allows the determination of stability for systems with feedback delays. The rationale for the method is explained in the Supplementary Methods VIII.1 and 2 and the stability limits are calculated in the Supplementary Methods VIII.3.

The analysis shows that the system can only be stabilized if *S<2*, and that for each value of *S*, there is a D-shaped region of feedback control parameters (G, D) that can stabilize the system (Figure 2.A). Feedback gain *G* must be greater than *S* to prevent falling, and smaller than a maximal value to avoid destabilizing the system. The behaviour of the system at minimal and maximal gain is illustrated in the Supplementary Methods VIII.4.

Likewise, the damping parameter *D* must be greater than the gain. As indicated by equation (1), this ensures that the feedback control counteracts the neural delay and acts as a function of the future position of the pendulum. If *D* is too large, the system enters into oscillations. The behaviour of the system at minimal and maximal damping is illustrated in the Supplementary Methods VIII.4.

Thus for each value of relative speed S, there is a limited range of feedback control parameters (G, D) that can stabilize the system. This analysis demonstrates that: 1) properties of feedback control must be adapted to the system's speed *S*, with lower gains for slower systems; 2) slower systems are more robust, in that the range of stable feedback parameters is larger.

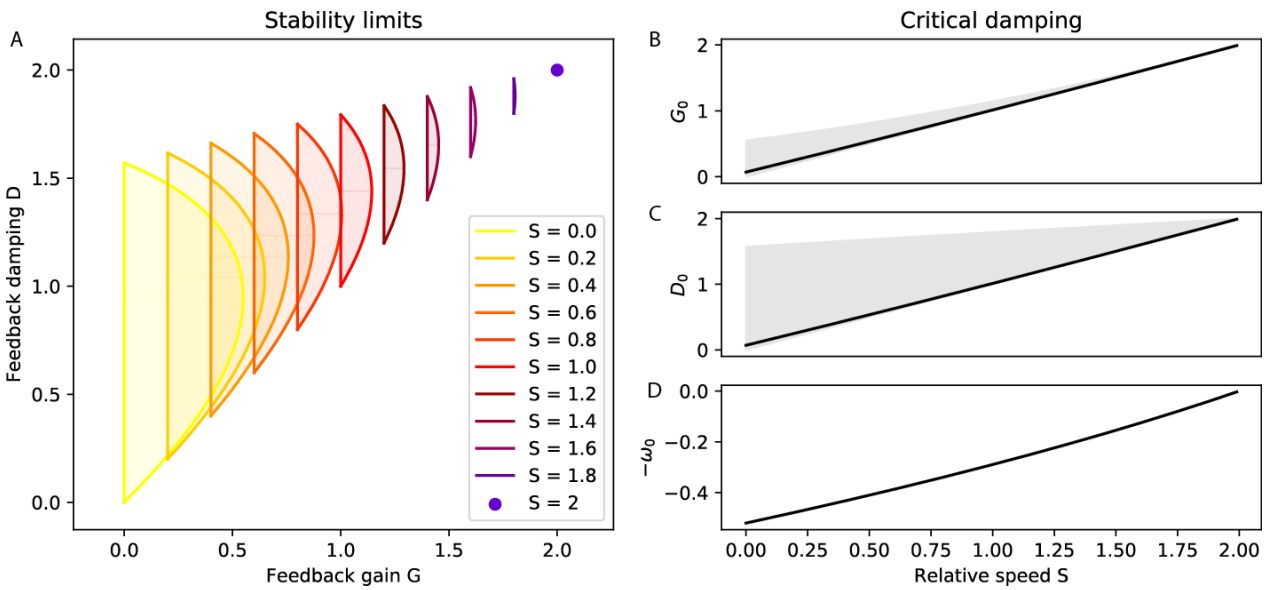

Figure 2 Delayed feedback control A. Stability limits. The range of stable feedback gain G and damping D is plotted for different values of relative speed S ranging from S = 0 to the maximal S = 2. B-D Optimal controller. B. The feedback gain G_0, which provides critical damping is plotted in black as a function of S. The range of stable feedback gains is shaded in grey. C. The feedback damping D_0, which provides critical damping is plotted in black as a function of S. The range of stable feedback damping is shaded in grey. D. The eigenvalue of the system with critical damping is plotted as a function of S; it corresponds to the inverse of the characteristic time of return to equilibrium

c. Best feedback gains

Within the range of stable feedback, large gain and low damping lead to oscillations, whereas low gain and large damping result in slow compensation for perturbations (as illustrated in the Supplementary Methods VIII.4). However, subjects typically adopt feedback gains that lead to fast compensation without oscillations (Bingham, Choi, & Ting, 2011). In second order systems governed by a characteristic equation $X^2 + 2\zeta\,\omega_0 X + \omega_0^2$, for a given value of ω_0, the fastest compensation without oscillations occurs for the critical damping $\zeta = 1$. For such critical damping, the characteristic equation has a unique double root $-\omega_0$ which captures the speed at which perturbations are attenuated: if a perturbation brings the system away from its equilibrium position, then the system is returned to its initial position following the time-course $\exp(-\frac{\omega_0 t}{\tau_{delay}})$. Higher damping results in slower compensation for perturbations, whereas lower damping results in oscillations.

To determine the best feedback gains for a given relative speed S, we used a linear approximation to the delay introduced by Pade (Hanta & Procházka, 2009). With this approximation, the characteristic equation becomes a third order polynomial (the details are provided in the Supplementary Methods IX.1). Then, we generalized the notion of critical damping to third order systems, considering that a system is critically damped when it has a unique triple eigenvalue (the details are provided in the Supplementary Methods IX.2). For each value of relative speed S, this procedure provided a unique value of control parameters (G_0, D_0) and eigenvalue $-\omega_0$, plotted in Figure 2.B-D.

We found that the optimal gain G_0 (Figure 2.B) and damping D_0 (Figure 2.C) are close to the minimal values required for stability. That is, $G_0 \approx D_0 \approx S$. This means that the gain is just large enough to prevent falling, and the damping is tuned so that the control depends on the predicted value of θ at the time after the feedback delay. It also implies that the best parameters are not the most robust, and therefore there might be a trade-off between fast stabilization and robustness. Moreover, both critical control parameters (G_0, D_0) increase with system speed. Finally, slower systems are stabilized more quickly by feedback (Figure 2.D).

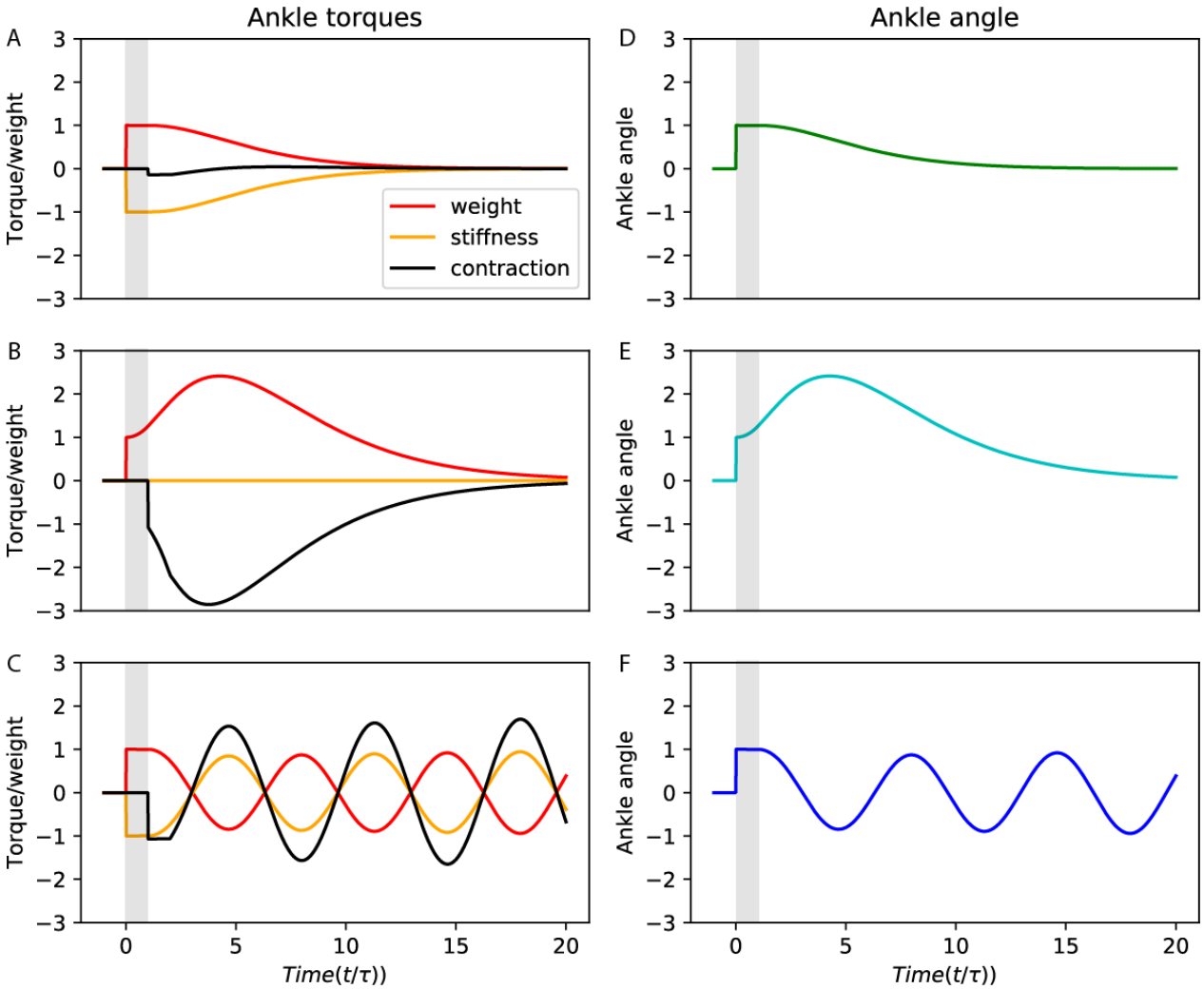

Figure 3 Response to perturbations. A. Response of a slow system S=0 with critical damping. B. Response of a fast system S=0.5 with critical damping. C. Response of a slow system S=0 with the same feedback controller as in B. The left panels show the time-course or the torque of weight (red), and the components of the ground reaction torque due to stiffness (orange) and feedback contraction (black), normalised to weight. The right panels show the time-course of ankle angle. The response delay (between the perturbation and the first change in contraction) is shaded in grey.

In Figure 3, we show the response of the inverted pendulum to an external perturbation occurring at time 0, which causes an initial shift in ankle angle by an arbitrary distance 1. We use mechanical parameters corresponding to human stance ($J \approx m\,L^2$, $L \approx 1\,m$, $cos(\theta_0) \approx 1$) and a time delay $\tau_{delay} \approx 0.3\,s$ as suggested for human stance (Ian D Loram & Lakie, 2002). We first consider a system with critical stiffness $k = mgLcos(\theta_0)$, such that $S = 0$. The response of the system with the best feedback gains is illustrated in Figure 3.A. The initial perturbation causes an immediate increase in the torque of weight, plotted in the left panel in red. Since ankle stiffness perfectly compensates for the torque of weight, there is an immediate, equivalent and opposite increase in the ground reaction torque component due to stiffness, plotted in the left panel in orange. Therefore, during the delay period (shaded in grey), the ankle angle (right panel) remains at a constant value. When the feedback control intervenes, a small increase in contraction (left panel, black) is sufficient to nudge the person back upright.

The response of the same system without ankle stiffness (such that $S = \tau_{delay}^2 \frac{mgLcos(\theta_0)}{J} = 0.5$) and with the best feedback gains is illustrated in Figure 3.B. The ground reaction torque component due to stiffness remains null (left panel, orange). During the delay period, the person therefore starts to fall, and picks up speed (right panel). When

the feedback control intervenes, a large increase in contraction is therefore necessary to first slow down falling, then return the ankle angle to its initial position. The fast system therefore requires large feedback parameters.

If the slow system is controlled with the feedback parameters appropriate for the fast system, then it is unstable (Figure 3.C). During the delay period, the person remains immobile. The large increase in contraction (left panel, black) then causes the ankle angle to overshoot its initial position, resulting in unstable oscillations (right panel).

Thus slower systems can be stabilized with less overshoot in ankle angle, and less change in muscle contraction, but require smaller feedback gains to prevent overshoot.

3) Generalisation to N dimensions

This analysis generalizes to the delayed feedback control of an N-dimensional system with interaction terms (and no mechanical damping) such as the arm (Hogan, 1985). The linearized dynamics of the system are given by:

$$\tau_{delay}{}^2 \frac{d^2}{dt^2}\begin{pmatrix}\theta_1\\ \cdots\\ \theta_N\end{pmatrix} = \begin{pmatrix}S_{1,1} & \cdots & S_{1,N}\\ \vdots & \ddots & \vdots\\ S_{N,1} & \cdots & S_{N,N}\end{pmatrix}\begin{pmatrix}\theta_1\\ \cdots\\ \theta_N\end{pmatrix} - \begin{pmatrix}C_1\\ \cdots\\ C_N\end{pmatrix}$$

$$\tau_{delay}{}^2 \ddot{\boldsymbol{\theta}} = \boldsymbol{S}\boldsymbol{\theta} - \mathbf{C}$$

where the control vector $\mathbf{C}$ is a delayed function of the variables $\theta_1, \cdots, \theta_N$ and their speeds $\dot{\theta}_1, \cdots, \dot{\theta}_N$.

In the generic case, the dynamics matrix $\boldsymbol{S}$ is diagonalisable, with eigenvalues $s_1, \cdots, s_N$. There is then a change of coordinates which transforms $\boldsymbol{\theta}$ to $\boldsymbol{\alpha}$ and $\mathbf{C}$ to $\mathbf{U}$ such that the system can be described as a set of N single-dimensional systems (see Supplementary Methods X):

$$\tau_{delay}{}^2 \frac{d^2}{dt^2}\alpha_i = s_i\alpha_i - U_i, i = 1 \dots N$$

For each such single-dimensional systems, the results of the previous section hold. Thus, the best stability is obtained when the relative speed s_i is smallest. Therefore, for multi-dimensional systems, the best stability is achieved when the body mechanical properties are adjusted so that all the eigenvalues of the dynamics matrix $\boldsymbol{S}$ are null. Additionally, the feedback gains must then be reduced to prevent overshoot.

4) Summary

We showed that the effect of body and environmental mechanical parameters and sensorimotor feedback delay can be captured by a dimensionless parameter S, which corresponds to how fast perturbations are amplified during the sensorimotor feedback delay. We then showed that this relative speed constrains the feedback gains that can stabilise the system. Slower systems are in a sense more robust, since they are stable over a wider range of feedback gains. We then proposed a novel method for calculating the best feedback gains for a system of a given speed, namely the feedback gains that provide the fastest cancellation of perturbations without overshoot. This allowed us to demonstrate that perturbations are cancelled faster in slower systems, provided feedback gains are reduced to prevent overshoot. We then generalised these results to multi-dimensional systems.

IV. Predictions and comparison to experiments

Our model thus predicts that, in order to improve motor stabilisation, subjects should adjust their body mechanical properties, such as stiffness, to decrease the amplification of perturbations during the response delay. Moreover, our model predicts that when subjects adopt this strategy, they must additionally decrease their neural feedback gains to prevent over-compensation. Here we show that our model accounts for motor stabilisation strategies adopted by humans both when standing in challenging balance conditions, and when manipulating unstable tools.

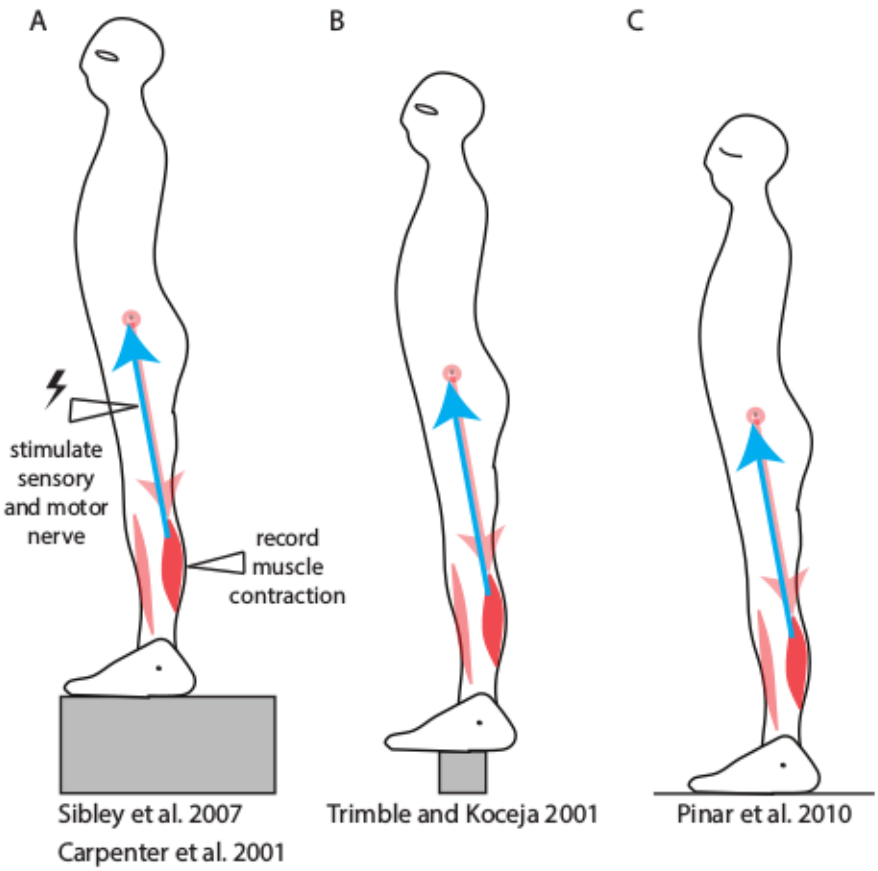

Figure 4 Decrease in soleus H-reflex in challenging balance conditions. Spinal feedback is probed by electrically stimulating the sensory fibres of a muscle and measuring the resulting change in muscle contraction, called the H-reflex. This H-reflex is larger in normal stance than A. when standing facing a cliff (Sibley et al. 2007), B. when standing on a narrow support (Trimble and Koceja 2001) and C. standing with the eyes closed (Pinar et al. 2010). Co-contraction of antagonist ankle muscles is observed in each of these three cases.

1) Quiet standing

When a subject is asked to stand in a situation in which it is particularly important not to move, an increase in ankle muscle co-contraction is observed, relative to normal stance. This occurs for example when standing facing a cliff as in Figure 4.A (Carpenter, Frank, Silcher, & Peysar, 2001), when standing on a narrow support as in Figure 4.B (Trimble & Koceja, 2001) or simply when closing the eyes as in Figure 4.C (Pinar et al., 2010). Increased co-contraction increases ankle stiffness (Nielsen et al., 1994). According to our model, this decreases the amplification of perturbations during the response delay, thereby improving stability.

Such a strategy additionally requires a decrease in neural feedback. The spinal feedback gain can be probed experimentally using the H-reflex (Knikou, 2008). This paradigm uses electrical stimulation of the calf muscle nerve to directly excite the sensory fibres embedded within the calf muscle (Figure 4.A, blue arrow), which are sensitive to the stretch of the calf muscle and therefore to ankle angle. In turn these sensory fibres directly excite the motor neurons of the ankle muscles, located in the spinal cord, which increase the contraction of the calf muscle (Figure 4.B, pink arrow). The change in muscle contraction for a given electrical stimulation is called the H-reflex. In the challenging balance conditions for which increased ankle muscle co-contraction is observed, there is additionally a decrease in the spinal H-reflex (Pinar et al., 2010; Sibley et al., 2007; Trimble & Koceja, 2001). We suggest that this decrease in spinal feedback is not indicative of an increased cortical control of posture, as commonly assumed, but is rather the hallmark of an increased reliance on body mechanics (namely ankle stiffness) for cancelling perturbations. In ballet dancers, which routinely practice balance in challenging situations, the spinal feedback gain

is reduced compared to normal subjects, even in normal balancing conditions, such as when standing on flat, solid ground (Mynark & Koceja, 1997). We suggest that this may be due to a long term adjustment of the properties of the ankle muscles and tendons, leading to an increased ankle stiffness, such as may be observed in long-distance runners (Kubo et al., 2015).

The human body comprises joints other than the ankle which are relevant for balance, such as the hip joint (Runge, Shupert, Horak, & Zajac, 1999). Our modelling results generalise to multi-dimensional systems and therefore predict that standing balance may also benefit from the stiffness of muscles acting at joints other than the ankle, if they slow down the amplification of perturbations during the response delay. This has indeed been shown by De Groote and colleagues, who asked human subjects to stand still despite external perturbations (De Groote et al., 2017). They observed the resulting motion of the body during the time it takes for the nervous system to intervene, and attempted to reproduce this motion in simulations. They found that if muscle stiffness was not included in their simulations, then the simulated body fell much faster than the human subjects. Thus, human leg muscles are arranged in such a way that muscle stiffness slows down falling. This suggests that further increases in the stiffness of leg muscles (through co-contraction) may be a useful strategy to further decrease falling speed.

2) Manipulation

Robustness to perturbations is also important for tool use (Rancourt & Hogan, 2001): for example, when manipulating a screwdriver, if forces perpendicular to the screwdriver's axis are applied on the handle, this may cause the screwdriver to slip from the screw (Figure 5.A). The task is inherently unstable in these lateral directions (in red in Figure 5.A), but inherently stable along the axis of the screwdriver (in green in Figure 5.A). Our modeling results predict that subjects compensate for tool instability by adjusting their arm mechanical properties to increase the stability of their arm specifically in the direction of tool instability.

The mechanical stability of the arm in a particular direction can be measured by having the subject hold on to a robotic handle, which applies an abrupt shift in handle position in that direction. The force the robot must exert to achieve this shift provides a measure of the arm stability in that direction, and is called arm endpoint stiffness (Burdet, Osu, Franklin, Milner, & Kawato, 2001). A theoretical study shows that arm endpoint stiffness depends both on arm posture, which affects the arm's inertia, and on the stiffness of the joints in the arm (Hogan, 1985). Subjects could therefore adjust their arm endpoint stiffness through adjustments of arm posture, and muscle co-contraction, which increases the stiffness of the joints.

An experimental paradigm has been developed to study the manipulation of tools in a laboratory setting (Burdet et al., 2001): a subject is asked to hold a handle, which is connected to a robotic arm. The robotic arm exerts forces that depend on the handle's position, and the pattern of forces is called the force field (Figure 5.B-H). Additionally, the robotic handle is used to apply the perturbations for measuring arm endpoint stiffness. Burdet and colleagues used a force field in which any lateral displacement of the hand elicits a lateral force proportional to the displacement (Burdet et al., 2001), as illustrated in Figure 5.B. This creates an instability when manipulating the handle, which is equivalent to the instability due to gravity when standing. They asked subjects to reach forwards with the handle to a target, and measured the arm endpoint stiffness in mid-reach. They showed that, after practicing reaching in this force field, subjects increased their endpoint stiffness, relative to reaching without a force field. Thus, subjects compensate for the object instability by actively adjusting the mechanical properties of their arm. Moreover, the authors showed that subjects increase their arm stiffness only in the lateral direction, which corresponds to the direction of instability of the force field, and not in the forwards direction. Darainy and colleagues then had subjects hold the handle at a given position in a laterally divergent force field (Figure 5.B), an antero-posteriorally divergent force field (Figure 5.C), or an isotropically divergent force field (Figure 5.D), and showed that in each case the subject increases their arm endpoint stiffness specifically in the direction of instability (Darainy, Malfait, Gribble, Towhidkhah, & Ostry, 2004). These studies demonstrate that subjects are able to actively adjust their arm endpoint stiffness in different directions. Our model accounts for the observations that subjects increase their arm endpoint stiffness specifically in the direction of the external instability.

One of the strategies used by subjects to adjust arm endpoint stiffness is increased muscle co-contraction. Thus, when subjects manipulate unstable objects, they increase both their arm muscle co-contraction and arm endpoint stiffness (Franklin, Osu, Burdet, Kawato, & Milner, 2003). This strategy is also used to improve pointing accuracy. Thus, Gribble and colleagues asked subjects to point at a given controlled speed to targets of different sizes (Gribble, Mullin, Cothros, & Mattar, 2003). Pointing to smaller targets requires more accurate reaching movements, and they observed that with decreasing target size, arm muscle co-contraction increased, the variability of the reach trajectories decreased, and the endpoint accuracy improved.

Another strategy used by subjects to adjust arm endpoint stiffness is the adjustment of arm posture. Thus, Trumbower and colleagues asked subjects to maintain different arm postures, and measured the arm endpoint stiffness for each of these postures (Trumbower et al., 2009). They showed that when the arm is extended forwards (Figure 5.E), the endpoint is stiff in the forwards but not in the lateral direction. Inversely, when the hand is kept close to the body (Figure 5.F), the endpoint is stiff in the lateral but not in the forwards direction. They then asked the subjects to track the position of a target in divergent force fields of different directions. In this task, the subjects were free to choose their arm posture, and the authors showed that in a forwards divergent force field, subjects extend their arm (Figure 5.E), whereas in a laterally divergent force field, they keep their arm close to the body (Figure 5.F). They thus adapted their arm posture to increase arm endpoint stiffness specifically in the direction of instability.

These experimental results therefore show that, as predicted by our model, subjects adjust their arm endpoint stiffness to compensate for external instabilities. This is achieved both through changes in muscle co-contraction and through changes in arm posture.

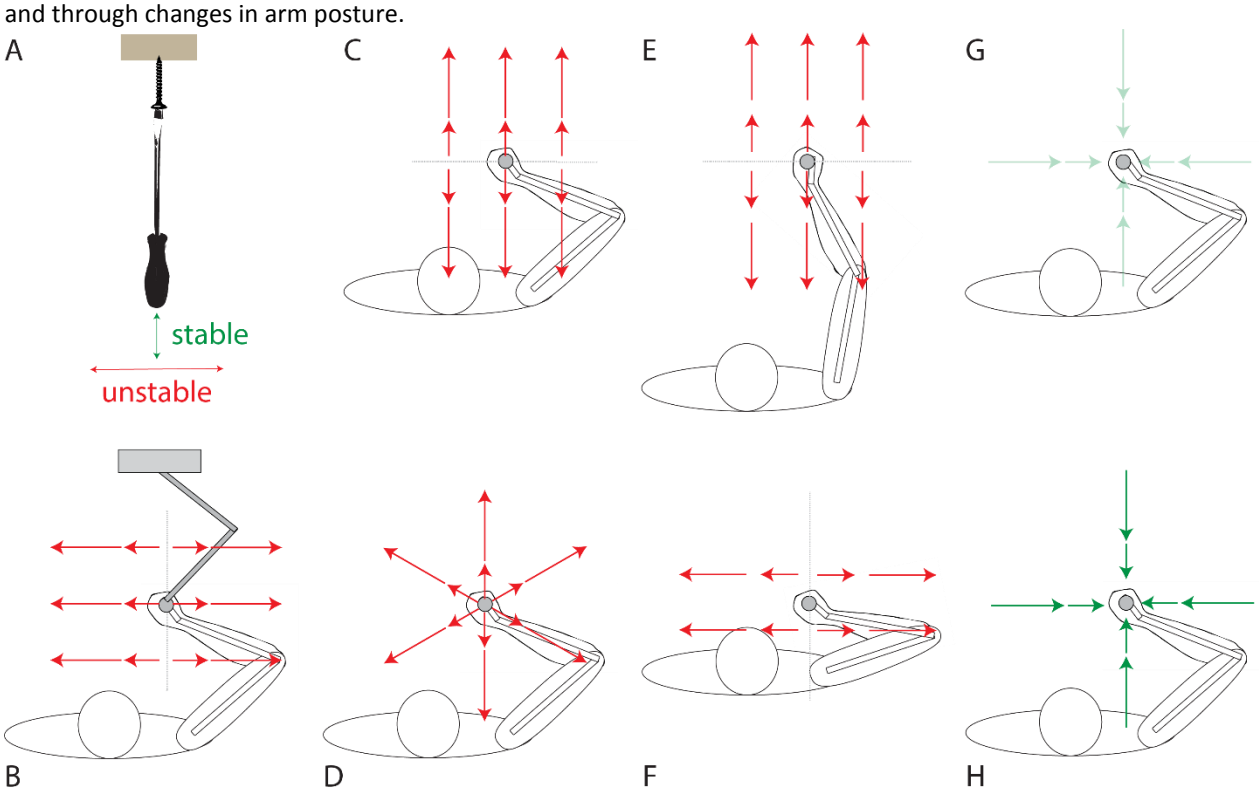

Figure 5 Tool manipulation A. Manipulating a screwdriver is inherently stable along the screw's axis (green) and unstable in perpendicular directions (red) (Rancourt & Hogan, 2001). B-D. When manipulating a tool that is unstable in the lateral direction (B), forwards direction (C) or that is isotropically unstable (D), subjects increase their arm endpoint stiffness specifically in the direction of instability (Burdet et al., 2001; Darainy et al., 2004). E-F. When subjects are free to adjust their arm posture, they extend the arm when manipulating a tool that is unstable in the forwards direction (E), but keep the arm close to the body when manipulating a tool that is unstable in the lateral direction (F); this increases arm endpoint stiffness specifically in the direction of instability (Trumbower et al., 2009). G-H. When manipulating a stable tool, the arm stretch reflex is reduced when the tool is stiff (H) rather than compliant (G) (Perreault, Chen, Trumbower, & Lewis, 2008).

Additionally, our model predicts that feedback gains are adapted to mechanical properties, such that feedback gains are reduced when arm endpoint stiffness is increased, to prevent over-compensation. This is also verified experimentally: Perreault and colleagues studied the manipulation of stable tools by having the robotic arm mimic a stiff handle (Perreault et al., 2008), with forces that return the handle to its reference position, whose amplitude is proportional to the distance to the reference position (Figure 5.G,H). These forces were either of small amplitude ("compliant" handle, Figure 5.G) or large amplitude ("stiff" handle, Figure 5.H). After the subjects had become used to the force field, the experimenter applied perturbations to the position of the handle, and measured the subject's muscular contraction response to the perturbation. The amplitude of the stretch reflex was smaller when manipulating the stiff handle rather than the compliant handle. In our model, this reduction in stretch reflex is necessary to avoid over-compensation.

V. Discussion

1) Anticipatory adjustment of mechanical properties for motor stabilisation

We present a generic model of stabilisation with neural response delays, which highlights the importance of the body mechanical properties for robustness to perturbations. We thus showed that the best stability is obtained when the body mechanical properties are adjusted so as to decrease the amplification of perturbations during the neural response delay. Our model therefore predicts that when immobility is particularly important, such as when manipulating an unstable tool, or when standing in challenging balance conditions, the appropriate strategy is to adjust the body mechanical properties to decrease this amplification, and additionally decrease the neural feedback gains. We then reviewed experimental evidence that young, healthy subjects can and do adopt this strategy. They achieve this either through increased co-contraction (Carpenter et al., 2001; Franklin et al., 2003; Gribble et al., 2003; Pinar et al., 2010; Trimble & Koceja, 2001), or through adjustments of arm posture (Trumbower et al., 2009). This allows them to actively adjust their limb stiffness and inertia, which should not be treated as fixed properties.

These properties determine the body's immediate response of the body to perturbations, therefore adjusting them in advance of perturbations provides the equivalent of a non-delayed feedback control, despite neural response delays. This strategy therefore combines the advantages of both feed-forward and feed-back compensation of perturbations: similarly to feed-forward control it bypasses the delays in neural intervention, however it does not require the precise advance knowledge of the perturbation which is typically assumed to be necessary for feedforward control (Shadmehr & Mussa-Ivaldi, 1994).

This strategy may explain the reduced variance in task-relevant dimensions, which is observed during skilled movement (Latash, Scholz, & Schöner, 2002; Scholz, Schöner, & Latash, 2000). For example, accurate aiming when shooting with a pistol requires the correct alignment of the pistol with the target. This can in principle be achieved with the shoulder and elbow more or less flexed, and indeed the observed variation in shoulder and elbow flexion from trial to trial is much larger than the variation in aiming, suggesting that elbow and shoulder flexion are coordinated to specifically reduce the variability in aiming direction (Scholz et al., 2000). To explain this task-appropriate pattern of variability, Latash and colleagues have put forward the "uncontrolled manifold hypothesis", which states that when attempting to achieve a task, the nervous system only corrects for deviations in the task-relevant dimension, allowing variation in the task-irrelevant dimensions to grow (Latash et al., 2002). Todorov and Jordan then suggested that the nervous system may achieve this through stochastic optimal feedback control (Todorov & Jordan, 2002). These authors thus attribute the reduction of variance in task-relevant dimensions to the neural feedback control of movement. However,as we have reviewed, subjects are able to modulate their body mechanical properties to improve stability specifically in the direction which is relevant to task success (Darainy et al., 2004). This improved mechanical stability would translate into reduced variability in that specific direction. We therefore suggest that the reduction of variability in task-relevant dimensions is due to the anticipatory adjustment of body mechanical properties, which reduces the amplification of perturbations in the task-relevant dimension. Testing this hypothesis can be done by probing how subjects respond to a change in task instruction. Subjects would be asked to maintain a robotic handle within a thin region oriented forwards (requiring high lateral precision) or laterally (requiring high forwards precision), and handle perturbations would be used to measure arm

endpoint stiffness and neural feedback gains in the lateral and forwards direction. We predict an increase in arm endpoint stiffness and a decrease in feedback gain in the task-relevant dimension; whereas the "uncontrolled manifold hypothesis" predicts an increase in feedback gain in the task-relevant dimension.

Moreover, subjects adjust their strategy to the task requirements. Thus, when Gribble and colleagues asked their subjects to point to smaller and smaller targets, they observed a decrease in trajectory variability and an increase in endpoint accuracy, as well as increased co-contraction (Gribble et al., 2003). Similarly, Franklin and colleagues asked subjects to reach in laterally divergent force fields of different strengths (Franklin, So, Kawato, & Milner, 2004), and showed that subjects increase their arm endpoint stiffness when manipulating more unstable objects. This strategy of adjusting the arm endpoint stiffness to the task requirements (such as targets of different sizes or handles with different instabilities) may underlie the speed-accuracy trade-off observed during reaching (Fitts, 1954). This could be tested by asking subjects to point to targets at different speeds, and measuring the arm endpoint stiffness for different reach speeds.

2) Is stability maximised?

Ankle stiffness during stance is measured by imposing a rotation of the ankle and measuring the immediate change in ground reaction torque that ensues. Experimental measures vary from 40% to 90% of the critical value $k_{crit} = mgL$ for which $S = 0$ (Casadio, Morasso, & Sanguineti, 2005; Lang & Kearney, 2014; Ian D. Loram et al., 2007; Vlutters, Boonstra, Schouten, & van der Kooij, 2015). The observation that ankle stiffness is typically lower than k_{crit} has given rise to a controversy on the relative importance of "passive" ankle stiffness and "active" neural feedback control for standing balance (Morasso & Sanguineti, 2002; Winter, Patla, Prince, Ishac, & Gielo-Perczak, 1998). Common to the two conflicting views is the assumption that ankle stiffness is a passive mechanical property. These approaches thus fail to take into consideration the subjects' ability to modulate ankle stiffness through ankle muscle co-contraction (Nielsen et al., 1994).

When standing in normal conditions, subjects typically do not co-contract their ankle muscles; however, they are able to do so when it is particularly important to remain immobile (Carpenter et al., 2001; Pinar et al., 2010; Trimble & Koceja, 2001). Likewise, during quiet standing, subjects continuously shift their position slightly over a range of around a centimetre; if however they are explicitly instructed to remain as still as possible, then this range is divided by two (I. D. Loram, Kelly, & Lakie, 2001). This suggests that in normal standing conditions, the standing posture is not adjusted to maximise stability (by imposing $S = 0$). We have indeed recently developed a theory of postural control (Le Mouel & Brette, 2017), according to which, during normal stance, posture is adjusted in view of mobility rather than immobility. This may induce subjects to adopt an ankle stiffness that is lower than the critical value. Indeed, maintaining a high ankle stiffness may prevent mobility, as it causes the ground reaction torque to immediately and mechanically cancel the torque of weight, whereas initiating a movement requires a net external torque to accelerate the movement (Le Mouel & Brette, 2017).

Similarly, during normal reaching, subjects do not typically maximise stability. Thus, when pointing to larger targets, subjects do not use the maximal co-contraction which they are capable of, and have larger trajectory variability and reduced endpoint accuracy compared to when reaching to smaller targets (Gribble et al., 2003). Similarly, when reaching in a laterally divergent force field of moderate strength, subjects do not adopt the maximal arm endpoint stiffness which they are capable of (Franklin et al., 2004). The authors suggest that this is because increased stiffness relies on muscle co-contraction, which may lead to fatigue.

Thus, during normal standing and reaching, stability is not maintained at its maximal possible value, possibly due to trade-offs with both mobility and fatigue. However, subjects can and do transiently increase their stability when this becomes important for motor performance, by adjusting the mechanical properties of their body in anticipation of the task.

VI. Competing interests

There are no competing interests.

VII. References

Aström, K. J., & Murray, R. M. (2010). *Feedback Systems: An Introduction for Scientists and Engineers*. Princeton University Press.

Bingham, J. T., Choi, J. T., & Ting, L. H. (2011). Stability in a frontal plane model of balance requires coupled changes to postural configuration and neural feedback control. *Journal of Neurophysiology*, *106*(1), 437–448.

Burdet, E., Osu, R., Franklin, D. W., Milner, T. E., & Kawato, M. (2001). The central nervous system stabilizes unstable dynamics by learning optimal impedance. *Nature*, *414*(6862), 446–449.

Carpenter, M. G., Frank, J. S., Silcher, C. P., & Peysar, G. W. (2001). The influence of postural threat on the control of upright stance. *Experimental Brain Research*, *138*(2), 210–218.

Casadio, M., Morasso, P. G., & Sanguineti, V. (2005). Direct measurement of ankle stiffness during quiet standing: implications for control modelling and clinical application. *Gait & Posture*, *21*(4), 410–424.

Darainy, M., Malfait, N., Gribble, P. L., Towhidkhah, F., & Ostry, D. J. (2004). Learning to Control Arm Stiffness Under Static Conditions. *Journal of Neurophysiology*, *92*(6), 3344–3350.

Duchateau, J., & Baudry, S. (2010). Training Adaptation of the Neuromuscular System. In P. V. Komi (Ed.), *Neuromuscular Aspects of Sport Performance* (pp. 216–253). Wiley-Blackwell.

Fitts, P. M. (1954). The information capacity of the human motor system in controlling the amplitude of movement. *Journal of Experimental Psychology*, *47*(6), 381–391.

Franklin, D. W., Osu, R., Burdet, E., Kawato, M., & Milner, T. E. (2003). Adaptation to Stable and Unstable Dynamics Achieved By Combined Impedance Control and Inverse Dynamics Model. *Journal of Neurophysiology*, *90*(5), 3270–3282.

Franklin, D. W., So, U., Kawato, M., & Milner, T. E. (2004). Impedance Control Balances Stability With Metabolically Costly Muscle Activation. *Journal of Neurophysiology*, *92*(5), 3097–3105.

Gribble, P. L., Mullin, L. I., Cothros, N., & Mattar, A. (2003). Role of Cocontraction in Arm Movement Accuracy. *Journal of Neurophysiology*, *89*(5), 2396–2405.

Hammond, P. H. (1956). The influence of prior instruction to the subject on an apparently involuntary neuro-muscular response. *The Journal of Physiology*, *132*(1), 17-18P.

Hanta, V., & Procházka, A. (2009). *Rational Approximation of Time Delay*.

Hogan, N. (1985). The mechanics of multi-joint posture and movement control. *Biological Cybernetics*, *52*(5), 315–331.

Knikou, M. (2008). The H-reflex as a probe: Pathways and pitfalls. *Journal of Neuroscience Methods*, *171*(1), 1–12.

Kubo, K., Miyazaki, D., Yamada, K., Yata, H., Shimoju, S., & Tsunoda, N. (2015). Passive and active muscle stiffness in plantar flexors of long distance runners. *Journal of Biomechanics*, *48*(10), 1937–1943. https://doi.org/10.1016/j.jbiomech.2015.04.012

Lang, C. B., & Kearney, R. E. (2014). Modulation of ankle stiffness during postural sway. In *2014 36th Annual International Conference of the IEEE Engineering in Medicine and Biology Society* (pp. 4062–4065).

Latash, M. L., Scholz, J. P., & Schöner, G. (2002). Motor control strategies revealed in the structure of motor variability. *Exercise and Sport Sciences Reviews*, *30*(1), 26–31.

Le Mouel, C., & Brette, R. (2017). Mobility as the Purpose of Postural Control. *Frontiers in Computational Neuroscience*, *11*, 67.

Le Mouel, C., Tisserand, R., Robert, T., & Brette, R. (2018). Anticipatory adjustments of posture allow elderly fallers to achieve a balance recovery performance equivalent to elderly non-fallers. *BioRxiv*.

Llewellyn, M., Yang, J. F., & Prochazka, A. (1990). Human H-reflexes are smaller in difficult beam walking than in normal treadmill walking. *Experimental Brain Research*, *83*(1), 22–28.

Loram, I. D., Kelly, S. M., & Lakie, M. (2001). Human balancing of an inverted pendulum: is sway size controlled by ankle impedance? *The Journal of Physiology*, *532*(Pt 3), 879–891.

Loram, Ian D, & Lakie, M. (2002). Human balancing of an inverted pendulum: position control by small, ballistic-like, throw and catch movements. *The Journal of Physiology*, *540*(Pt 3), 1111–1124. https://doi.org/10.1113/jphysiol.2001.013077

Loram, Ian D., Maganaris, C. N., & Lakie, M. (2007). The passive, human calf muscles in relation to standing: the non-linear decrease from short range to long range stiffness. *The Journal of Physiology*, *584*(Pt 2), 661–675.

McGeer, T. (1990). Passive Dynamic Walking. *The International Journal of Robotics Research*, *9*(2), 62–82.

Michiels, W., & Niculescu, S. (2007). *Stability and Stabilization of Time-Delay Systems*. Society for Industrial and Applied Mathematics.

Morasso, P. G., & Sanguineti, V. (2002). Ankle Muscle Stiffness Alone Cannot Stabilize Balance During Quiet Standing. *Journal of Neurophysiology*, *88*(4), 2157–2162. https://doi.org/10.1152/jn.2002.88.4.2157

Mynark, R. G., & Koceja, D. M. (1997). Comparison of soleus H-reflex gain from prone to standing in dancers and controls. *Electroencephalography and Clinical Neurophysiology*, *105*(2), 135–140.

Nielsen, J., Sinkjær, T., Toft, E., & Kagamihara, Y. (1994). Segmental reflexes and ankle joint stiffness during co-contraction of antagonistic ankle muscles in man. *Experimental Brain Research*, *102*(2), 350–358. https://doi.org/10.1007/BF00227521

Nyquist, H. (1932). Regeneration theory. *The Bell System Technical Journal*, *11*(1), 126–147. https://doi.org/10.1002/j.1538-7305.1932.tb02344.x

Perreault, E. J., Chen, K., Trumbower, R. D., & Lewis, G. (2008). Interactions With Compliant Loads Alter Stretch Reflex Gains But Not Intermuscular Coordination. *Journal of Neurophysiology*, *99*(5), 2101–2113.

Pinar, S., Kitano, K., & Koceja, D. M. (2010). Role of vision and task complexity on soleus H-reflex gain. *Journal of Electromyography and Kinesiology: Official Journal of the International Society of Electrophysiological Kinesiology*, *20*(2), 354–358.

Pruszynski, J. A., & Scott, S. H. (2012). Optimal feedback control and the long-latency stretch response. *Experimental Brain Research*, *218*(3), 341–359.

Rancourt, D., & Hogan, N. (2001). Stability in Force-Production Tasks. *Journal of Motor Behavior*, *33*(2), 193–204.

Runge, C. F., Shupert, C. L., Horak, F. B., & Zajac, F. E. (1999). Ankle and hip postural strategies defined by joint torques. *Gait & Posture*, *10*(2), 161–170.

Scholz, J. P., & Schöner, G. (1999). The uncontrolled manifold concept: identifying control variables for a functional task. *Experimental Brain Research*, *126*(3), 289–306.

Scholz, J. P., Schöner, G., & Latash, M. L. (2000). Identifying the control structure of multijoint coordination during pistol shooting. *Experimental Brain Research*, *135*(3), 382–404.

Shadmehr, R., & Mussa-Ivaldi, F. A. (1994). Adaptive representation of dynamics during learning of a motor task. *The Journal of Neuroscience: The Official Journal of the Society for Neuroscience*, *14*(5 Pt 2), 3208–3224.

Sibley, K. M., Carpenter, M. G., Perry, J. C., & Frank, J. S. (2007). Effects of postural anxiety on the soleus H-reflex. *Human Movement Science*, *26*(1), 103–112.

Sproewitz, A., Tuleu, A., Vespignani, M., Ajallooeian, M., Badri, E., & Ijspeert, A. (2013). Towards Dynamic Trot Gait Locomotion—Design, Control and Experiments with Cheetah-cub, a Compliant Quadruped Robot. *International Journal of Robotics Research*, *32*(8), 932–950. https://doi.org/10.1177/0278364913489205

Todorov, E., & Jordan, M. I. (2002). Optimal feedback control as a theory of motor coordination. *Nature Neuroscience*, *5*(11), 1226–1235.

Trimble, M. H., & Koceja, D. M. (2001). Effect of a reduced base of support in standing and balance training on the soleus H-reflex. *The International Journal of Neuroscience*, *106*(1–2), 1–20.

Trumbower, R. D., Krutky, M. A., Yang, B.-S., & Perreault, E. J. (2009). Use of Self-Selected Postures to Regulate Multi-Joint Stiffness During Unconstrained Tasks. *PLoS ONE*, *4*(5).

Vlutters, M., Boonstra, T. A., Schouten, A. C., & van der Kooij, H. (2015). Direct measurement of the intrinsic ankle stiffness during standing. *Journal of Biomechanics*, *48*(7), 1258–1263.

Welch, T. D. J., & Ting, L. H. (2008). A Feedback Model Reproduces Muscle Activity During Human Postural Responses to Support-Surface Translations. *Journal of Neurophysiology*, *99*(2), 1032–1038. https://doi.org/10.1152/jn.01110.2007

Winter, D. A., Patla, A. E., Prince, F., Ishac, M., & Gielo-Perczak, K. (1998). Stiffness control of balance in quiet standing. *Journal of Neurophysiology*, *80*(3), 1211–1221.

VIII. Supplementary methods: Stability analysis

The system is a linearized inverted pendulum, with an external forcing F:

$$\tau_{delay}{}^2\ddot{\theta} - S\,\theta = F \tag{2}$$

The system is controlled with delayed proportional-derivative feedback u, based on the observed value of θ, written θ_{obs}:

$$u = (G\theta_{obs} + D\tau_{delay}\dot{\theta}_{obs})\big(t - \tau_{delay}\big) \tag{3}$$

To determine the stability of the system, we analyze how perturbation signals propagate through the system. we consider 2 types of perturbation: a perturbation δ in the external force, and noise η in the observation process:

$$F = -u + \delta$$
$$\theta_{obs} = \theta + \eta$$

The block diagram of the controlled system with noise is shown in Figure 6.A.

Replacing in (2) and (3):

$$\tau_{delay}{}^2\ddot{\theta} - S\,\theta = \delta - G\theta(t-\tau) - D\tau_{delay}\,\dot{\theta}(t-\tau) - G\eta(t-\tau) - D\tau_{delay}\,\dot{\eta}(t-\tau)$$
$$\tau_{delay}{}^2\ddot{\theta} - S\,\theta + G\theta(t-\tau) + D\tau_{delay}\,\dot{\theta}(t-\tau) = \delta - G\eta(t-\tau) - \tau_{delay}D\,\dot{\eta}(t-\tau) \tag{4}$$

The unforced motion of the system (for $\delta = 0$ and $\eta = 0$) is given by the solutions to the homogeneous equation:

$$\tau_{delay}{}^2\ddot{\theta} - S\,\theta + G\theta(t-\tau) + D\tau_{delay}\,\dot{\theta}(t-\tau) = 0$$

The solutions to this equation are called the modes of the system. After an arbitrary perturbation, the unforced motion of the system is a weighted sum of such modes.

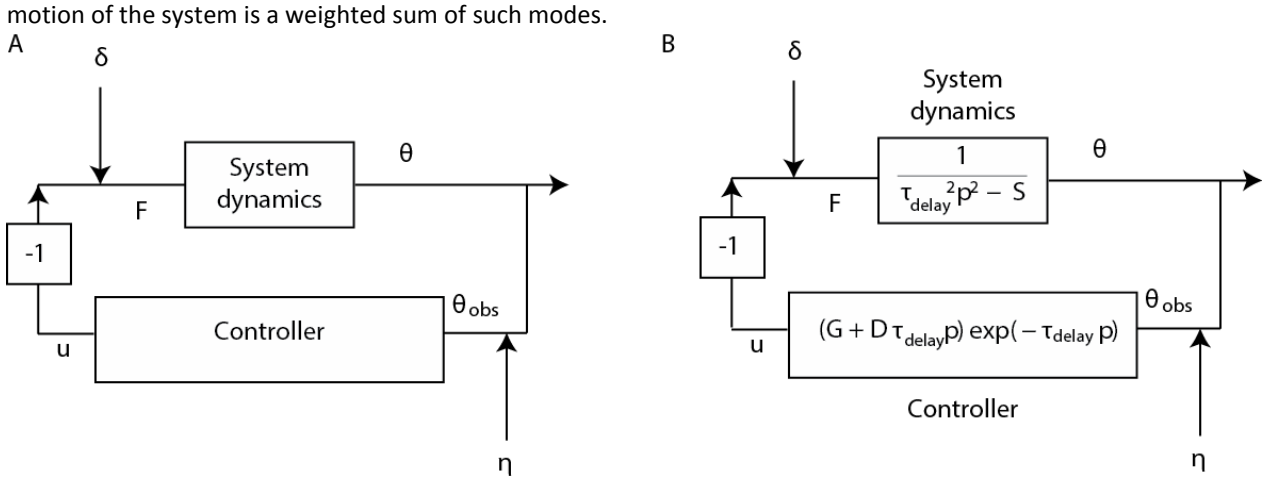

Figure 6 Block diagram of the controlled system

A. Noise is injected into the system both at the level of the motor command (δ) and at the level of the sensory feedback (η). B. Transfer function of the system dynamics and controller.

1) Propagation of exponential signals and derivation of the characteristic equation

Since the system is linear, we only need to consider the response to exponential signals e^{pt} where p is a complex number. The response to a sum of exponential signals is then the sum of the responses to each exponential signal. I therefore consider perturbations of the form:

$$\delta(t) = \delta_0 e^{pt}$$
$$\eta(t) = \eta_0 e^{pt}$$

Then the response of the system is also an exponential signal such that:

$$\theta(\mathrm{t}) = \theta_0 e^{pt}$$

The transfer function of the system dynamics and controller are shown in Figure 6.B.

Replacing in (4):

$$\left({\tau_{delay}}^2 p^2 - S + G e^{-p\tau_{delay}} + D\tau_{delay} p e^{-p\tau_{delay}}\right) \theta_0 e^{pt} = \delta_0 e^{pt} - \left(G + D\tau_{delay} p\right) e^{-p\tau_{delay}} \eta_0 e^{pt}$$

The solutions to the characteristic equation $D(p) = 0$ correspond to the modes of the homogeneous equation, where:

$$D(p) = {\tau_{delay}}^2 p^2 - S + G e^{-p\tau_{delay}} + D\tau_{delay} p e^{-p\tau_{delay}}$$

If there exists p with positive real part such that $D(p) = 0$, then the system is unstable. Indeed, the amplitude of an exponential signal is $e^{Re(p)t}$, thus if $Re(p) > 0$ the amplitude of the mode grows exponentially with time. If this mode is excited by a perturbation at one point, then even after the end of the perturbation, the system will diverge.

This can also be seen by looking at the transfer function of the system:

$$\theta_0 = \frac{\delta_0 - (G + D\tau_{delay} p) e^{-p\tau_{delay}} \eta_0}{{\tau_{delay}}^2 p^2 - S + (G + D\tau_{delay} p) e^{-p\tau_{delay}}}$$

If $D(p) = 0$, then the response of the system to a perturbation e^{pt} diverges, since the denominator of the transfer function becomes zero. The roots of the denominator are called the poles. The system is therefore stable if and only if its transfer function has no poles with positive real part (Aström & Murray, 2010).

Note that the denominator is the same whether noise in injected into the motor or the sensory process. The system is therefore either robust to both sensory and motor noise or robust to neither. Indeed, stability only depends on the behaviour of the homogeneous equation.

The difficulty in assessing stability comes from the feedback delay, which introduces the $e^{-p\tau_{delay}}$ term: because of this term, the characteristic equation has an infinite number of roots, and there is no straightforward criterion to determine stability (Michiels & Niculescu, 2007). Consider for example, the characteristic equation $1 + e^{-p\tau_{delay}} = 0$. For all integers n, $p = \frac{i(1+2n)\pi}{\tau_{delay}}$ is a root of the equation: the equation therefore has an infinite number of roots.

To assess stability, we will therefore use the Nyquist criterion, introduced by Nyquist (Nyquist, 1932) and described in the following section. For convenience, we will apply the Nyquist to the open-loop transfer function:

$$OL(p) = \frac{\left(G + D\tau_{delay} p\right) e^{-\tau_{delay} p}}{{\tau_{delay}}^2 p^2 - S}$$

The transfer function of the system is related to the open loop transfer function according to:

$$\theta_0 = \frac{\frac{\delta_0}{{\tau_{delay}}^2 p^2 - S} - OL(p)\eta_0}{1 + OL(p)}$$

The poles of the transfer function are therefore the zeros of $1 + OL(p)$.

2) Nyquist criterion

I therefore seek to determine whether $f(p) = 1 + OL(p)$ has zeros with positive real part.

For this, we will use Cauchy's residue theorem, which states that the integral of a function $g(p)$ (which must be analytical except at a number of poles and zeros) over a contour in the complex plane is equal to the sum of the residues of $g(p)$ at each of its poles and zeros within the region encompassed by that contour.

I first introduce the function $g(p) = \frac{f\prime(p)}{f(p)}$ whose sum of residues within a region is equal to the difference between the number of zeros and poles of $f(p)$ within that region. we then integrate this function over the Nyquist contour which encompasses the right half-plane. we thus determine the number of zeros of $f(p)$ with positive real part.

a. Residues of g(p)

The function $g(p) = \frac{f\prime(p)}{f(p)}$ is analytical except at the poles and zeros of $f(p)$.

I therefore use Cauchy's residue theorem, which states that the integral of $g(p)$ over a contour Γ is equal to the sum of the residues of $g(p)$ at each of its poles and zeros within this contour (which correspond to the poles and zeros of $f(p)$).

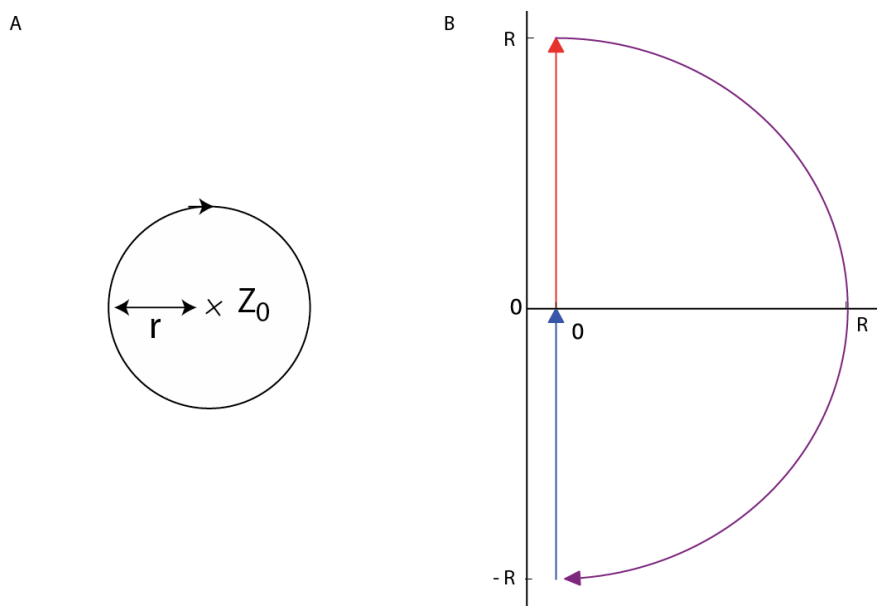

Figure 7 Calculation of residuals within the Nyquist contour

A. Neighbourhood of a zero or pole B. D-shaped contour of a given radius R

Zeros

I consider z_0 a zero of $f(p)$ of multiplicity m, and write:

$$f(p) = (p - z_0)^m h(p)$$

$$g(p) = \frac{f'(p)}{f(p)} = \frac{m(p - z_0)^{m-1} h(p)}{(p - z_0)^m h(p)} + \frac{(p - z_0)^m h'(p)}{(p - z_0)^m h(p)}$$

$$= \frac{m}{p - z_0} + \frac{h'(p)}{h(p)}$$

There exists a neighbourhood of z_0 for which $h(p)$ and therefore $\frac{h\prime(p)}{h(p)}$ is analytic. We choose r such that the circle Γ_{r,z_0} centered at z_0 and of radius r is contained within this neighbourhood (Figure 7.A). The residue of $g(p)$ at z_0 is equal to the integral of $g(p)$ around the circle:

$$Res(z_0) = \oint_{\Gamma_{r,z_0}} g(p)dp = \oint_{\Gamma_{r,z_0}} \frac{m}{p - z_0} dp + \oint_{\Gamma_{r,z_0}} \frac{h'(p)}{h(p)} dp$$

Since $\frac{h\prime(p)}{h(p)}$ is analytic within this circle:

$$\oint_{\Gamma_{r,z_0}} \frac{h'(p)}{h(p)} dp = 0$$

I introduce the change of variables: $p = z_0 + re^{i\phi}, dp = ire^{i\phi} d\phi$

$$\oint_{\Gamma_{r,z_0}} \frac{m}{p - z_0} dp = m \int_{\phi=0}^{2\pi} \frac{ire^{i\phi} d\phi}{re^{i\phi}} = 2i\,\pi\,m$$

Poles

I consider p_0 a pole of $f(p)$ of multiplicity n, and write:

$$f(p) = \frac{k(p)}{(p - p_0)^n}$$

$$f'^{(p)} = \frac{k'(p)}{(p - p_0)^n} + k(p)(-n)\frac{1}{(p - p_0)^{n+1}}$$

$$g(p) = \frac{f'(p)}{f(p)} = \frac{k'(p)}{k(p)} - \frac{n}{p - p_0}$$

There exists a neighbourhood of p_0 for which $k(p)$ is analytic. The residue of $g(p)$ at p_0 is equal to the integral of $g(p)$ around the circle Γ_{r,p_0} centred on p_0 and included within this neighbourhood:

$$\oint_{\Gamma_{r,p_0}} \frac{-n}{p - p_0} dp = -2\,i\,\pi\,n$$

Therefore, the integral of $g(p)$ over the a contour is equal to $2i\,\pi\,(m - n)$, where m is the number of zeros of $f(p)$ and n is the number of poles of $f(p)$ within that contour.

b. Nyquist contour

Since the region we am interested in is the entire right half-plane (the region of the complex plane with positive real part), we will use the Nyquist contour Γ_N, which is the limit, for $R \to +\infty$, of the D-shaped contour (traversed counterclockwise) defined by:

- $i\omega$ for ω ranging from $-R$ to $+R$
- $R\,e^{i\,\phi}$ for ϕ ranging from π/2 to - π/2

This contour is plotted in Figure 7.B for a given radius R, and for $R \to +\infty$ this contour encompasses all of the complex plane with positive real part. Note: we use the convention that clockwise curves are oriented positively.

c. Geometrical interpretation

$$\oint_{\Gamma_N} g(p)dp = \oint_{\Gamma_N} \frac{f'(p)}{f(p)} dp = \oint_{\Gamma_N} \frac{d}{dp} \log\big(f(p)\big)\, dp = \oint_{\Gamma_N} \frac{d}{dp} \log(|f(p)|)\, dp + \oint_{\Gamma_N} \frac{d}{dp} i \arg\big(f(p)\big)\, dp$$

The variation of $|f(p)|$ over the closed contour Γ_N is zero.
The number of zeros minus poles is therefore equal to the winding number w:

$$w = \frac{1}{2\,\pi} \oint_{\Gamma_N} \frac{d}{dp} \arg\big(f(p)\big)\, dp$$

Geometrically, w corresponds to the number of clockwise loops effected by $f(p)$ around 0 when p ranges over the Nyquist curve.

The Nyquist criterion thus states that a system described by the open-loop transfer function $OL(p)$ with n poles with positive real part is stable if and only if the curve described by $OL(p)$, as p ranges over the Nyquist contour, loops n times counter-clockwise around the point -1.

3) Application to our system

The open-loop transfer function is given by:

$$OL(p) = \frac{\big(G + D\tau_{delay} p\big) e^{-\tau_{delay} p}}{{\tau_{delay}}^2 p^2 - S}$$

$f(p) = 1 + OL(p)$ has a unique pole with positive real part $p = \sqrt{S}/\tau_{delay}$. Therefore, the system is stable if and only if the integral of $g(p)$ over the Nyquist contour is equal to $-2i\,\pi$. Thus, for the system to be stable, the open-loop transfer function $OL(p)$ must loop once counterclockwise around the point -1 when p ranges over the Nyquist contour.

The second part of the Nyquist contour, defined by $R\, e^{i\,\phi}$ for ϕ ranging from π/2 to - π/2, with $R \to +\infty$, maps onto the point 0. Indeed:

$$\lim_{R \to +\infty} OL\big(R\, e^{i\,\phi}\big) = 0$$

The first part of the Nyquist contour, defined by $i\omega$ for ω ranging from $-\infty$ to $+\infty$, maps onto the curve described by:

$$OL(i\omega) = \frac{\big(G + D\tau_{delay} i\omega\big) e^{-\tau_{delay} i\omega}}{-{\tau_{delay}}^2 \omega^2 - S}$$

I introduce the dimensionless parameter:

$$X = \tau_{delay}\omega$$

Then the Nyquist curve can equivalently be described by (with X ranging from $-\infty$ to $+\infty$):

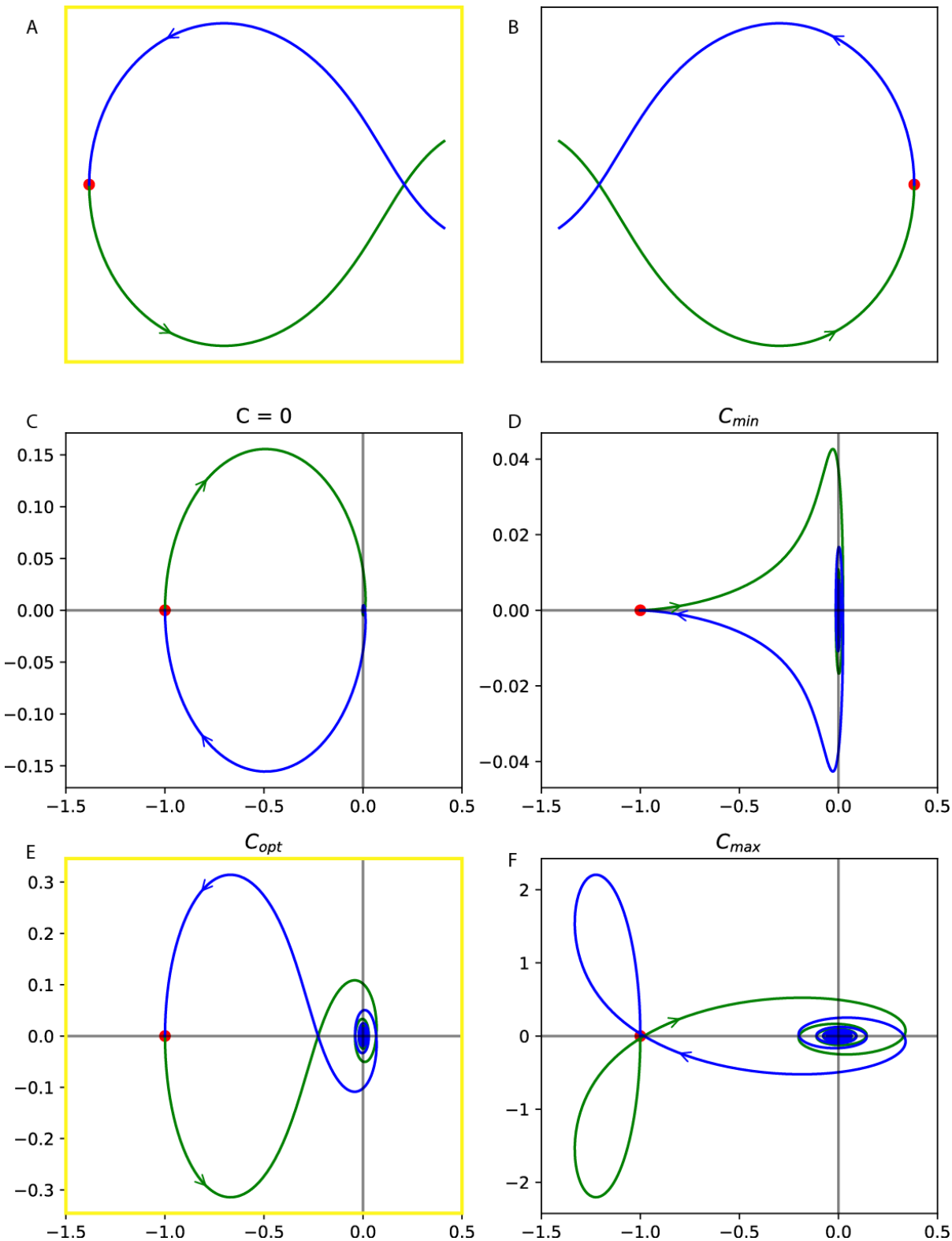

Figure 8 Nyquist curves.

The Nyquist curve is plotted in blue for X < 0, in green for X > 0, and in red for X = 0. Two possibilities for a counterclockwise loop are schematically illustrated in A. and B. The Nyquist curve is plotted for C = 0 in panel C., minimal damping C = 1 in panel D., critical damping C_{opt} in panel E., and maximal damping C_{max} in panel F. The only curve in panels C-F which contains a counterclockwise loop is the one in panel E, which corresponds to the situation in panel A.

$$OL(X) = -\frac{(G + iDX)e^{-iX}}{X^2 + S}$$

To disentangle the effects of G, D and S on stability, we introduce $C = \frac{D}{G}$ such that the gain G simply scales the curve defined by:

$$OL(X) = -G\frac{(1 + iCX)e^{-iX}}{X^2 + S}$$

I first determine the parameters (S, C) for which there exists a counterclockwise loop in the curve. For clarity, in figures we use the gain $G = S$. Then, for a given set of admissible (S, C), we determine the minimal and maximal gains for which the curve loops around -1.

a. $(\boldsymbol{S}, \boldsymbol{C})$ parameters with a counter-clockwise loop

Description of the curve:

- The curve for $X < 0$ is the symmetric with respect to the real axis of the curve for $X > 0$
- For $X = \pm\infty$, $OL = 0$ because of the X^2 in the denominator
- For $X = 0$, $OL = -G/S$

I consider the first intersection point of the Nyquist curve with the real axis for $X > 0$, and denote it $X_{int}(C, S)$. There are 2 options for a counter-clockwise loop, schematically illustrated in Figure 8:

A. $-G/S < OL(X_{int}(C, S))$ and the imaginary part is negative for $X \in [0, X_{int}(C, S)]$ (Figure 8.A)
B. $-G/S > OL(X_{int}(C, S))$ and the imaginary part is positive for $X \in [0, X_{int}(C, S)]$ (Figure 8.B)

Determination of the intersection point

I expand the open-loop into real and imaginary parts:

$$OL(X) = -G\frac{(1 + iCX)(\cos(X) - i\sin(X))}{X^2 + S} = \frac{G}{X^2 + S}(1 + iCX)(-\cos(X) + i\sin(X))$$

$$= \frac{G}{X^2 + S}(-(\cos(X) + CX\sin(X)) + i(-CX\cos(X) + \sin(X)))$$

The sign of the imaginary part is thus the same as the sign of:

$$I(C, X) = -CX\cos(X) + \sin(X)$$

This function is illustrated in Figure 9.A for different values of C. The intersection point therefore depends only on C and not on S, and we write it $X_{int}(C)$. It satisfies :

$$\frac{\tan(X_{int}(C))}{X_{int}(C)} = C$$

As can be seen in Figure 9.A:

- For $C < 1$, $X_{int}(C) \in]\pi/2, 3\pi/2[$ and $I(C, X) > 0$ for $X \in [0, X_{int}(C)]$
- For $C > 1$, $X_{int}(C) \in]0, \pi/2[$ and $I(C, X) < 0$ for $X \in [0, X_{int}(C)]$

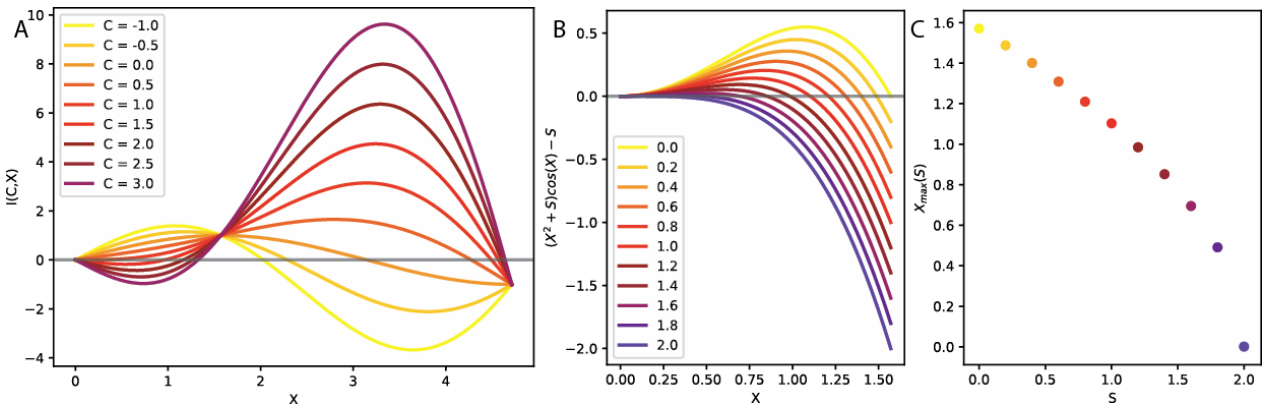

Figure 9 Determination of the intersection point.

A. The curve I(C,X) is illustrated as a function of X for different values of C ranging from -1 to 3. B. The curve $f_S(X)$ is illustrated as a function of X for different values of S ranging from 0 to 2. C. The maximal value of the intersection point X for which there exists a counterclockwise loop in the Nyquist curve is illustrated as a function of S.

Indeed, a first order expansion around $X = 0$ gives:

$$I(C, X) \propto -CX + X = X(1 - C)$$

I now consider the value of the open-loop function at the intersection point:

$$OL(X_{int}) = \frac{-G}{{X_{int}}^2 + S}(\cos(X_{int}) + CX_{int}\sin(X_{int})) = \frac{-G}{{X_{int}}^2 + S}\frac{1}{\cos(X_{int})}(\cos(X_{int})^2 + \sin(X_{int})^2)$$
$$= \frac{-G}{({X_{int}}^2 + S)\cos(X_{int})}$$

Stability requires C > 1

As we have shown, for $C < 1$, $X_{int}(D) \in]\pi/2, 3\pi/2[$ therefore $\cos(X_{int}) < 0$ and $OL(X_{int}) > 0 > -G/S$. Moreover, for $C < 1$, the imaginary part is positive for $X \in [0, X_{int}(D)]$. Thus, the Nyquist curve satisfies neither conditions A. nor conditions B., and the system is not stable: there is no counter-clockwise loop in the curve. The Nyquist curves for $C = 0$ and $C = 1$ are illustrated in Figure 8 (respectively panel C. and D.).

Stability requires $S < 2$

As we have shown, for $C > 1$, the imaginary part is negative for $X \in [0, X_{int}(C)]$. Stability therefore requires satisfying condition A., ie:

$$-\frac{G}{S} < OL\big(X_{int}(C)\big) = \frac{-G}{(X_{int}(C)^2 + S)\cos\big(X_{int}(C)\big)}$$
$$0 < (X_{int}(C)^2 + S)\cos\big(X_{int}(C)\big) - S$$

$X_{int}(C)$ is an increasing function of C, ranging from 0 for $C \to 1$ to $\frac{\pi}{2}$ for $C \to +\infty$.

I therefore define $f_S: X \in \left[0, \frac{\pi}{2}\right] \to (X^2 + S)\cos(X) - S$

$$f_S(0) = 0$$
$$f_S\left(\frac{\pi}{2}\right) = -S$$

This function is illustrated in Figure 9.B for different values of S.

The derivative is given by:

$$f_s'(X) = 2X\cos(X) - S\sin(X)$$

For $S \geq 2$, it is negative throughout the range $\left[0, \frac{\pi}{2}\right]$, therefore $f_s(X)$ is also negative throughout this range (Figure 9.B), and there exists no value of C for which the system is stable.

Stability requires $C < C_{max}(S)$
For $S < 2$, $f_s'(0) > 0$, therefore there exists a range of values $X \in [0, X_{max}(S)]$ for which $f_S(X) > 0$. The value of $X_{max}(S)$ for different values of S is shown in Figure 9.C. Thus there exists a range of $C \in [1, C_{max}(S)]$ for which the Nyquist curve has a counterclockwise loop. $C_{max}(S)$ is given by:

$$C_{max}(S) = \frac{\tan(X_{max}(S))}{X_{max}(S)}$$

The Nyquist curve for the critical damping $C_{opt} > 1$ (as derived in the following section V.2) and the maximal value of damping $C_{max}(S)$ are illustrated in Figure 8 (respectively panel E. and F.)

b. Feedback gain G for which the loop encompasses -1

Finally, for a given value of speed and damping, the range of gains which can stabilize the system is given by:

$$-\frac{G}{S} < -1 < \frac{-G}{(X_{int}(C)^2 + S)\cos(X_{int}(C))}$$
$$S < G < (X_{int}(C)^2 + S)\cos(X_{int}(C))$$

The minimal gain is thus $G = S$ for all values of C.
The maximal gain depends on C, and follows a curve parametrized by $X \in [0, X_{max}(S)]$:

$$G = (X^2 + S)\cos(X)$$
$$C = \frac{\tan(X)}{X}$$

Note that $G(0) = S$ and $G(X_{max}(S)) = S$.

4) Simulations

a. Feedback gain G

The response of systems with various feedback gains is shown in Figure 10.A for the relative speed $S = 0.1$ and the critical damping D_{opt} for that relative speed (derived in the following section V):

- For $G < S$ (dashed red line), the feedback is not strong enough to prevent falling, and the system is unstable.
- For $G = S$ (dashed black line), the feedback is just strong enough to prevent falling, but not strong enough to bring the system back to its initial position: this is the lower limit of stability.
- For $G = G_{max}$ (full black line), the feedback elicits oscillations whose amplitude neither increases nor decreases with time: this is the upper limit of stability.

For gains between S and G_{max} (blue and green dashed and full lines), the system is stable:

- For $G = G_{opt}$ the critical gain (full green line) the perturbation is cancelled the fastest without oscillations.
- For $G < G_{opt}$ (dashed blue line), the perturbation is cancelled more slowly.
- For $G > G_{opt}$ (full blue line), there are oscillations.

b. Feedback damping D

The response of systems with various feedback dampings is shown in Figure 10.B, for the relative speed $S = 0.1$ and the critical gain G_{opt}. If the damping is too low (dashed red and black lines), slow oscillations appear, whereas if

it is too large (full black line), fast oscillations appear. For intermediate values of damping (full and dashed blue and green lines), the perturbation is cancelled the fastest without oscillations for $D = D_{opt}$ (full green line).

c. Relative speed S

The response of systems with various relative speeds and critical feedback parameters is shown in Figure 10.C:

- As S approaches 2 (blue line), an initial perturbation of amplitude 1 is amplified 400 times before it is cancelled by the feedback (note the difference in the scale of the y axis between panel C and panels A and B).
- For $S = 2$ (black line), the amplitude of the oscillations neither increases nor decreases with time: this is the upper limit of stability.
- For $S > 2$ (red line), no feedback gains are able to stabilize the system, and the amplitude of the oscillations grows with time.

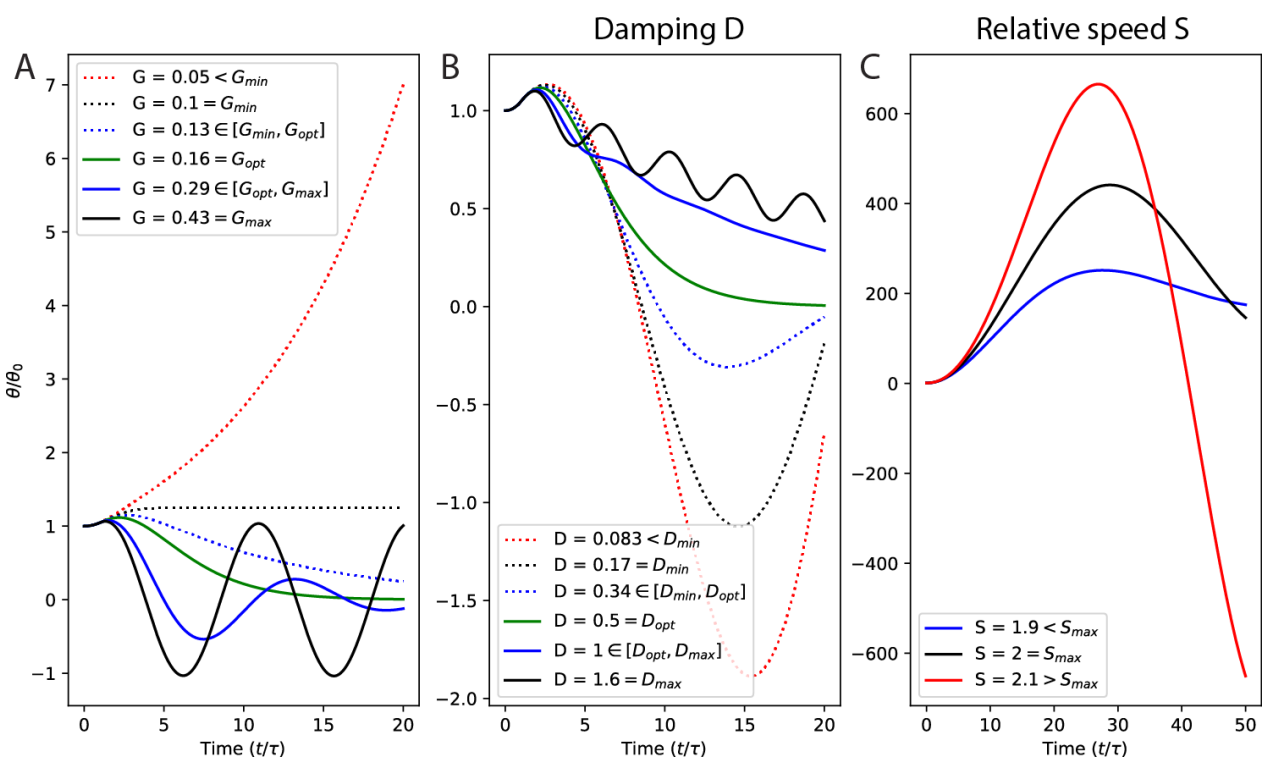

Figure 10 Response to a perturbation.

The position ϑ of the system to a perturbation of arbitrary magnitude ϑ_0 is displayed as a function of time (normalized to the response delay τ_{delay}). A. Response of a system with relative speed S = 0.1, damping D_{opt} (S), and various gains. B. Response of a system with relative speed S = 0.1, gain G_{opt} (S), and various dampings. C. Response of the system with various relative speeds, and critical gain and damping G_{opt} (S),D_{opt} (S). Stable systems are in blue and green, unstable systems in red, and systems at the border of stability in black. Systems with feedback parameters lower than the critical values are in dashed lines.

IX. Supplementary methods: Critical damping

Critical damping is defined for second order systems governed by a characteristic equation of the form:

$$X^2 + 2\zeta\,\omega_0 X + \omega_0^2$$

The characteristic equation of the linearized inverted pendulum with delayed feedback control is:

$$X^2 - S + Ge^{-X} + DXe^{-X}$$

To define critical damping for this system, we first introduce a rational function approximation for the delay. With this approximation, the characteristic equation becomes a third order polynomial. we then generalize the notion of critical damping from second order to third order polynomials.

1) Pade approximation

a. Rational function approximation

The first order Pade approximation of the delay is given by:

$$e^{-X} = \frac{e^{-X/2}}{e^{X/2}} \approx \frac{1 - X/2}{1 + X/2}$$

With this approximation, the characteristic equation becomes

$$X^2 - S + Ge^{-X} + DXe^{-X} \approx (X^2 - S) + (G + DX)\frac{1 - X/2}{1 + X/2}$$

$$= \frac{1}{1 + \frac{X}{2}}((X^2 - S)\left(1 + \frac{X}{2}\right) + (G + DX)\left(1 - \frac{X}{2}\right))$$

$$= \frac{1}{1 + \frac{X}{2}}(\frac{X^3}{2} + X^2\left(1 - \frac{D}{2}\right) + X\left(D - \frac{G}{2} - \frac{S}{2}\right) + G - S)$$

The roots of the approximate characteristic equation are thus the roots of:

$$X^3 + X^2(2 - D) + X(2D - G - S) + 2(G - S)$$

b. Dynamical systems interpretation

The Pade approximation consists in approximating the function $\theta(t - \tau_{delay})$ by a function $\theta_{approx}(t)$ which follows:

$$\frac{\tau_{delay}}{2}\dot{\theta}_{approx}(t) + \theta_{approx}(t) = \theta(t) - \frac{\tau_{delay}}{2}\dot{\theta}(t) \tag{5}$$

Examples

Suppose $\theta(t)$ is a step function defined by (Figure 11.A. in black):

- $\theta(t) = 0 \; for \; t < 0$
- $\theta(t) = 1 \; for \; t > 0$

Then $\theta_{approx}(t) = 1 - \exp(-\frac{2t}{\tau_{delay}})$ (Figure 11.A. in red).

Suppose $\theta(t)$ is a sinusoidal function defined by $\theta(t) = \exp(i\omega t)$ (Figure 11.B, C, in black), then:

$$\theta_{approx}(t) = \frac{1 - \frac{i\omega\tau_{delay}}{2}}{1 + \frac{i\omega\tau_{delay}}{2}}\exp(i\omega t)$$

The amplitude is:

$$\sqrt{\frac{(1 + (\frac{\omega\tau_{delay}}{2})^2)^2}{(1 + (\frac{\omega\tau_{delay}}{2})^2)^2}} = 1$$

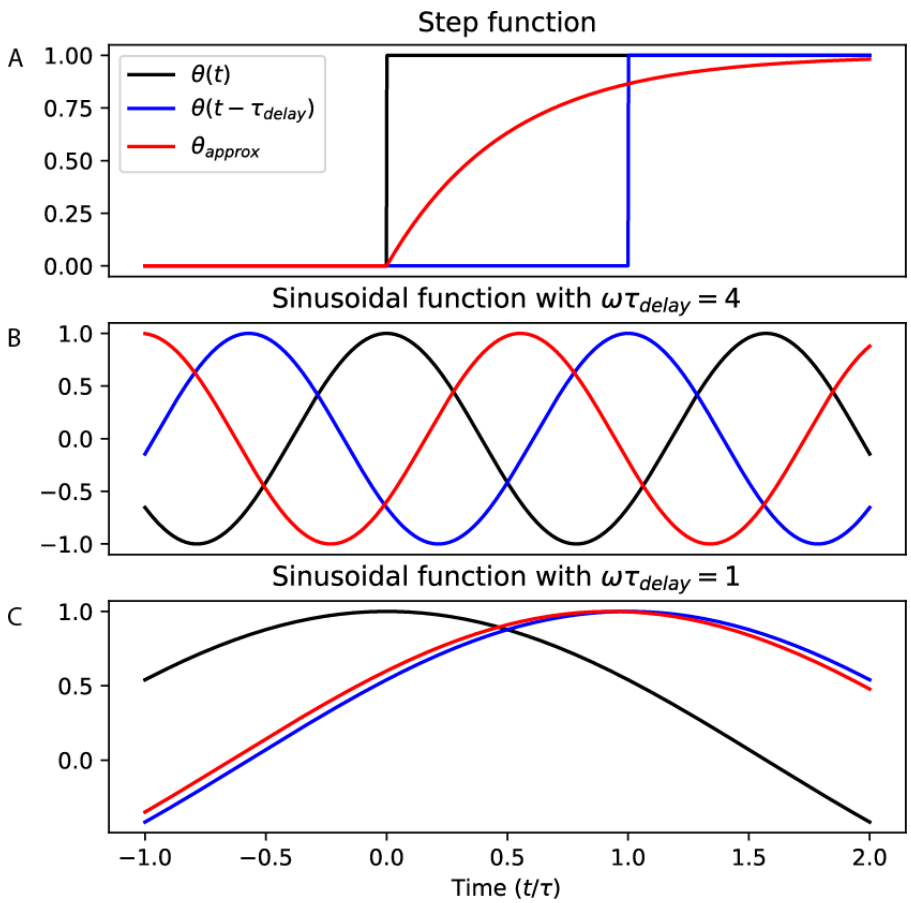

Figure 11 Pade approximation of the time delay.

A. Step function in black, delayed step function in blue and Pade approximation of the delayed step function in red. B-C Sinusoidal function with $\omega\tau_{delay} = 4$ and 1 (respectively for panels B and C) in black, delayed sinusoidal function in blue and Pade approximation of the delayed sinusoidal function in red.

The phase lag is:

$$\phi\left(\frac{1-\frac{i\omega\tau_{delay}}{2}}{1+\frac{i\omega\tau_{delay}}{2}}\right) = -2\arctan\left(\frac{\omega\tau_{delay}}{2}\right)$$

This corresponds to a time lag of τ_{delay} for small $\omega\tau_{delay}$ (Figure 11.C in red) and π for large $\omega\tau_{delay}$ (Figure 11.B in red).

Thus, the Pade approximation $\theta_{approx}(t)$ corresponds to $\theta(t-\tau_{delay})$ if θ changes slowly compared to τ_{delay} (Figure 11.C), whereas fast variations in θ are distorted (Figure 11.A, B).

Delayed feedback control

With this approximation, the dynamics of the system with delayed feedback control become:

$$\tau_{delay}{}^2\ddot{\theta} = S\,\theta - \left(G\theta + D\dot{\theta}\right)(t-\tau_{delay}) \approx S\,\theta - \left(G\theta_{approx} + D\dot{\theta_{approx}}\right) \qquad (6)$$

Reinjecting equation (5) into (6):

$$\tau_{delay}{}^2\ddot{\theta} \approx S\,\theta - G\theta_{approx} - D(2\theta - 2\theta_{approx} - \tau_{delay}\dot{\theta})$$
$$\tau_{delay}{}^2\ddot{\theta} \approx (S-2D)\theta + (2D-G)\theta_{approx} + D\,\tau_{delay}\dot{\theta}$$

$$\tau_{delay}\frac{d}{dt}\begin{pmatrix}\theta\\ \theta_{approx}\\ \tau_{delay}\dot{\theta}\end{pmatrix}=\begin{pmatrix}0 & 0 & 1\\ 2 & -2 & -1\\ S-2D & (2D-G) & D\end{pmatrix}\begin{pmatrix}\theta\\ \theta_{approx}\\ \tau_{delay}\dot{\theta}\end{pmatrix}$$

The eigenvalues of the system are the roots of the polynomial:

$$X^3+X^2(2-D)+X(2D-G-S)+2(G-S)$$

2) Generalisation of criticality

a. Definition

In second order systems governed by a characteristic equation $X^2+2\zeta\,\omega_0 X+\omega_0^2$, for a given value of ω_0, the fastest compensation without oscillations occurs for the critical damping $\zeta=1$. For such critical damping, the characteristic equation has a unique double root $-\omega_0$. Higher damping results in slower compensation for perturbations, whereas lower damping results in oscillations.

I generalize the notion of 'critical damping', and consider that a third order system is likewise critically damped when it has a unique triple negative root $-\omega_0$. The coefficients of the characteristic equation must therefore correspond to the coefficients of the polynomial:

$$(X+\ \omega_0)^3=X^3+X^2 3\omega_0+X\,3{\omega_0}^2+{\omega_0}^3$$

b. Solution

For a given speed S, we solve for $(\omega_0, \mathrm{G_{opt}}, \mathrm{D_{opt}})$ the system of equations:

$$0={\omega_0}^3-2(\mathrm{G_{opt}}-S) \qquad (7)$$
$$0=3{\omega_0}^2-(2\mathrm{D_{opt}}-\mathrm{G_{opt}}-S) \qquad (8)$$
$$0=3\omega_0-(2-\mathrm{D_{opt}}) \qquad (9)$$

First we determine ω_0 as a function of S by removing (G,D) from the equations:
According to (9): $\mathrm{D_{opt}}=2-3\omega_0$
According to (8): $\mathrm{G_{opt}}=2D-S-3{\omega_0}^2=4-6\omega_0-S-3\,{\omega_0}^2$
Replacing in (7):

$$0={\omega_0}^3-8+12\,\omega_0+2S+6{\omega_0}^2+2S=\ {\omega_0}^3+6{\omega_0}^2+12\,\omega_0+4S-8=(\omega_0+2)^3-8+4S-8$$

Thus: $(\omega_0+2)^3=4(4-S)>0$
This equation admits one real positive solution for (ω_0+2), and two complex conjugate solutions. we take the real solution:

$$\omega_0=\ -2+(16-4S)^{\frac{1}{3}}$$

Replacing in (5): $\mathrm{D_{opt}}=2-3\omega_0=8-3(16-4S)^{\frac{1}{3}}$
Replacing in (4):$\mathrm{G_{opt}}=4-6\omega_0-S-3\,{\omega_0}^2=4+12-6(16-4S)^{\frac{1}{3}}-S-3(4+(16-4S)^{\frac{2}{3}}-4(16-4S)^{\frac{1}{3}})$

$$\mathrm{G_{opt}}=4-S+6(16-4S)^{\frac{1}{3}}-3(16-4S)^{\frac{2}{3}}$$

X. Supplementary methods: generalisation to N dimensions

I consider an N-dimensional dynamical system with state $\boldsymbol{\theta}$ and delayed feedback control $\mathbf{C}$, whose dynamics are governed by:

$$\tau_{delay}{}^2 \frac{d^2}{dt^2}\begin{pmatrix}\theta_1\\ \cdots\\ \theta_N\end{pmatrix} = \begin{pmatrix}S_{1,1} & \cdots & S_{1,N}\\ \vdots & \ddots & \vdots\\ S_{N,1} & \cdots & S_{N,N}\end{pmatrix}\begin{pmatrix}\theta_1\\ \cdots\\ \theta_N\end{pmatrix} - \begin{pmatrix}C_1\\ \cdots\\ C_N\end{pmatrix}$$

$$\tau_{delay}{}^2 \ddot{\boldsymbol{\theta}} = \boldsymbol{S}\boldsymbol{\theta} - \mathbf{C}$$

I consider that the transpose $\boldsymbol{S}^T$ of the dynamics matrix $\boldsymbol{S}$ is diagonalizable, and introduce the basis set $(\boldsymbol{e_1}, \dots, \boldsymbol{e_N})$ of eigenvectors of $\boldsymbol{S}^T$ and their corresponding eigenvalues $(s_1, \dots, s_N)$, such that for every i:

$$\boldsymbol{S}^T \boldsymbol{e_i} = s_i \boldsymbol{e_i}$$

I use this basis set to perform a transformation of coordinates of the state $\boldsymbol{\theta}$ into $\boldsymbol{\alpha}$, such that, for every i, α_i is the dot product of the vectors $\boldsymbol{e_i}$ and $\boldsymbol{\theta}$:

$$\alpha_i = \boldsymbol{e_i}^T\, \boldsymbol{\theta}$$

Each component α_i follows the dynamical equation:

$$\tau_{delay}{}^2 \frac{d^2}{dt^2}\alpha_i = \boldsymbol{e_i}^T \boldsymbol{S}\boldsymbol{\theta} - \boldsymbol{e_i}^T \mathbf{C} = s_i \boldsymbol{e_i}\boldsymbol{\theta} - \boldsymbol{e_i}^T \mathbf{C} = \mathrm{s_i}\alpha_i - \boldsymbol{e_i}^T \mathbf{C}$$

The dynamics are thus decomposed into a set of N components, each of which follows a single-dimensional dynamics for which the analysis presented in section II.1, 2 holds. Stability is thus determined by the set of eigenvalues of $\boldsymbol{S}^T$, which corresponds to the set of eigenvalues of $\boldsymbol{S}$.